

Interannual Rainfall Extremes over Southwest Western Australia Linked to Indian Ocean Climate Variability

MATTHEW H. ENGLAND, CAROLINE C. UMMENHOFER, AND AGUS SANTOSO

Centre for Environmental Modelling and Prediction, School of Mathematics, University of New South Wales, Sydney, Australia

(Manuscript received 15 December 2004, in final form 24 August 2005)

ABSTRACT

Interannual rainfall extremes over southwest Western Australia (SWWA) are examined using observations, reanalysis data, and a long-term natural integration of the global coupled climate system. The authors reveal a characteristic dipole pattern of Indian Ocean sea surface temperature (SST) anomalies during extreme rainfall years, remarkably consistent between the reanalysis fields and the coupled climate model but different from most previous definitions of SST dipoles in the region. In particular, the dipole exhibits peak amplitudes in the eastern Indian Ocean adjacent to the west coast of Australia. During dry years, anomalously cool waters appear in the tropical/subtropical eastern Indian Ocean, adjacent to a region of unusually warm water in the subtropics off SWWA. This dipole of anomalous SST seesaws in sign between dry and wet years and appears to occur in phase with a large-scale reorganization of winds over the tropical/subtropical Indian Ocean. The wind field alters SST via anomalous Ekman transport in the tropical Indian Ocean and via anomalous air–sea heat fluxes in the subtropics. The winds also change the large-scale advection of moisture onto the SWWA coast. At the basin scale, the anomalous wind field can be interpreted as an acceleration (deceleration) of the Indian Ocean climatological mean anticyclone during dry (wet) years. In addition, dry (wet) years see a strengthening (weakening) and coinciding southward (northward) shift of the subpolar westerlies, which results in a similar southward (northward) shift of the rain-bearing fronts associated with the subpolar front. A link is also noted between extreme rainfall years and the Indian Ocean Dipole (IOD). Namely, in some years the IOD acts to reinforce the eastern tropical pole of SST described above, and to strengthen wind anomalies along the northern flank of the Indian Ocean anticyclone. In this manner, both tropical and extratropical processes in the Indian Ocean generate SST and wind anomalies off SWWA, which lead to moisture transport and rainfall extremes in the region. An analysis of the seasonal evolution of the climate extremes reveals a progressive amplification of anomalies in SST and atmospheric circulation toward a wintertime maximum, coinciding with the season of highest SWWA rainfall. The anomalies in SST can appear as early as the summertime months, however, which may have important implications for predictability of SWWA rainfall extremes.

1. Introduction

The Australian continent experiences high interannual climate variability, particularly in precipitation rates (Power et al. 1998; Drosowsky 1993a). Rainfall over southwest Western Australia (SWWA) shows unique characteristics in temporal variability (Smith et al. 2000) and evidence of an overall decline during winter over the past century (Allan and Haylock 1993; Ansell et al. 2000b). On shorter time scales, interannual variability of SWWA rainfall remains poorly under-

stood, as traditional predictors for Australian climate, such as the Southern Oscillation index, appear to resolve little of the region's variability (Smith et al. 2000). Several studies have revealed a connection between Indian Ocean sea surface temperature (SST) and Australian rainfall (e.g., Nicholls 1989; Frederiksen and Balgovind 1994; Reason et al. 1998; Li and Mu 2001; Qian et al. 2002). However, these previous studies relate to the large-scale mean Australian or Western Australian rainfall. The focus of our study is on the more localized region of SWWA and more specifically the interannual rainfall variability over the southwestern tip of Western Australia (region shown in Fig. 1a). Of particular interest is how the SWWA interannual rainfall variability might be controlled by the adjacent Indian Ocean.

Relatively few studies have focused on the natural

Corresponding author address: Matthew H. England, Centre for Environmental Modelling and Prediction, School of Mathematics, University of New South Wales, Sydney, 2052 Australia.
E-mail: M.England@unsw.edu.au

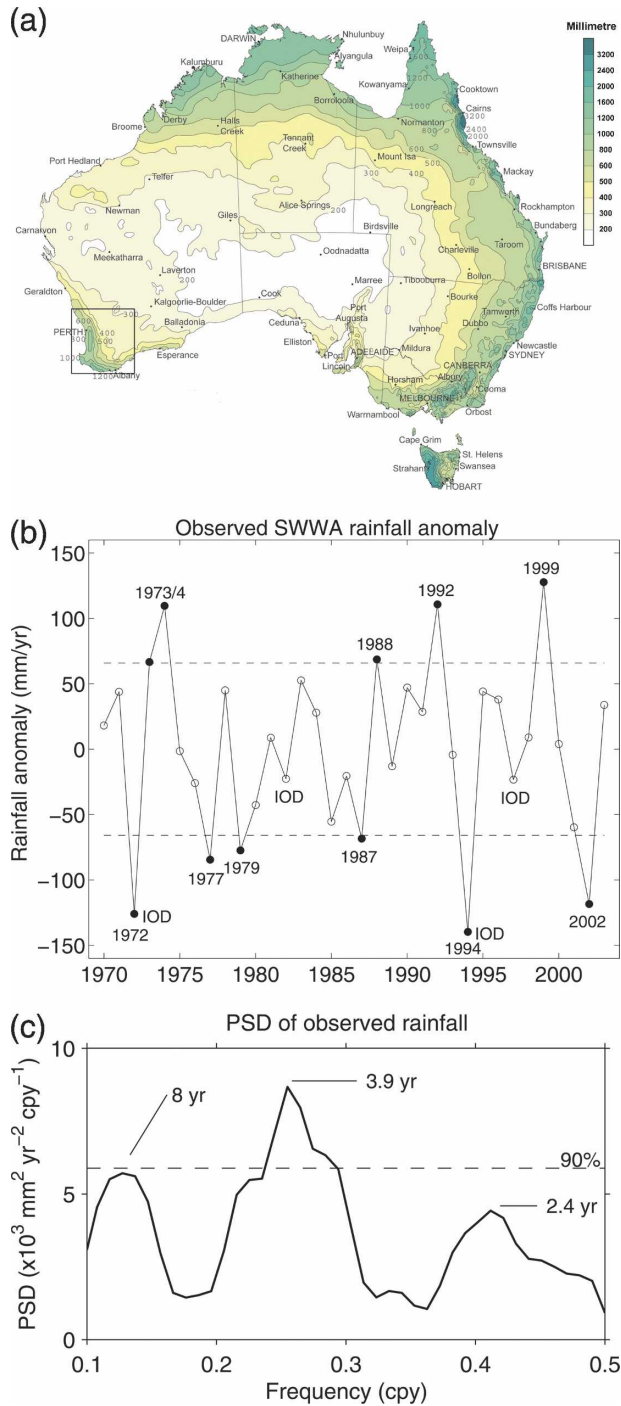


FIG. 1. (a) Annual precipitation (mm yr^{-1}) over Australia from the BoM gridded rainfall climatology, with the study area in SWWA indicated (30° – 35° S, 115° – 120° E). (b) Detrended time series (solid line) of the observed annual rainfall anomaly (mm yr^{-1}) for SWWA for 1970–2003; dashed lines indicate \pm one standard deviation (66 mm yr^{-1}) and years with rainfall exceeding this are marked as extremes (filled circles). Years identified by Saji et al. (1999) as IOD years for the period 1970–99 are also indicated (1972, 1982, 1994, and 1997). (c) PSD of observed SWWA precipitation using the Thomson multitaper method (Mann and Lees 1996). The dashed horizontal line represents the estimated white noise spectrum at the 90% confidence level.

year-to-year variability of rainfall over SWWA. Ansell et al. (2000b) used empirical orthogonal functions of monthly data to show that SWWA winter rainfall is significantly correlated with winter SST over the subtropical Indian Ocean over the period 1907–94. However, they found that the links between rainfall and SST are less significant than those for mean sea level pressure (MSLP) and rainfall. Similarly, Smith et al. (2000) investigated observations and reanalyses for the period 1950–94 and found a relationship between SWWA rainfall and SST in the tropical southeast and midlatitude Indian Ocean. Again, these were found to be less robust than those seen using MSLP. Allan and Haylock (1993) use gridded station data for the period 1911–89 to show that SWWA winter rainfall anomalies may be associated with fluctuations in midlatitude frontal systems, resulting from modulation in the semipermanent longwave (anticyclone) trough south of Australia. This modulation is caused by interactions between Indian Ocean SST anomalies and the overlying atmosphere. Allan and Haylock (1993) and Smith et al. (2000), among other studies, also focus on a long-term winter rainfall decline over SWWA over the past 40 yr. The cause of this multidecadal shift in SWWA rainfall remains a topic of debate. For example, the Indian Ocean Climate Initiative (IOCI 2002) attribute the decrease in winter rainfall in the mid-1970s to an increase in air pressure at 30° – 50° S, which forces large-scale atmospheric circulation changes in the region. The IOCI (2002) suggest that these changes may have been forced by increasing atmospheric greenhouse gases. Further evidence of a greenhouse fingerprint in SWWA rainfall decline has recently been provided in the climate change simulations of Cai et al. (2003), who show that increasing CO_2 can force a century-scale decline in winter rainfall. In contrast, Pitman et al. (2004) suggest that the rainfall decline and coinciding temperature increase is mostly due to large-scale changes in SWWA land cover over the past 50 yr. They use a model to demonstrate that cleared vegetation patterns result in an increased moisture divergence over SWWA and a corresponding enhanced moisture convergence inland. In the present study, however, we focus on the shorter time-scale interannual variability and extend previous studies by evaluating over 30 yr of observations and reanalysis data, as well as interannual SWWA rainfall variability in a multicentury coupled climate model.

The tropical Indian Ocean is characterized by a seasonal reversal of the zonal monsoon winds and a resulting seasonal tilt of the thermocline. A positive air–sea thermal feedback between an anomalous atmospheric anticyclone and a cold SST anomaly can result in Indian

Ocean Dipole (IOD) events in certain years (Saji et al. 1999; Li et al. 2003; Yamagata et al. 2003; Saji et al. 2005). These appear as a pattern of internal Indian Ocean variability with negative SST anomalies off Indonesia and anomalously high SST in the western Indian Ocean, accompanied by changes in zonal wind strength over the equator (Saji et al. 1999). A positive air–sea feedback is set up, reinforcing the anomalous state, until the seasonal reversal of the wind field across the equatorial Indian Ocean counteracts it, leading to a rapid decline of the IOD event. The close relationship between zonal winds and SST indicates strong air–sea coupling over the tropical Indian Ocean (e.g., Rao et al. 2002; Ashok et al. 2003a; Li et al. 2003; Iizuka et al. 2000). Recently, IOD events have been associated with low Australian rainfall due to anomalous anticyclonic circulation over the eastern Indian Ocean and Australia, resulting in anomalous subsidence over the Australian continent (Ashok et al. 2003b; Saji and Yamagata 2003a). Of the rainfall extremes normally associated with Indian Ocean SST variability, especially in the form of the IOD, most studies concentrate on its effect on Indian (Ashok et al. 2001; Li et al. 2003; Ashok et al. 2004b), Indonesian (Saji et al. 1999), and African (Reason 1999; Saji et al. 1999; Black 2003) precipitation. One exception is the study by Ashok et al. (2003b), who focus on a link between the IOD and Australian winter rainfall using 20 yr of observations and results from an atmospheric GCM. Here, we extend this by analyzing interannual rainfall variability over southwest Western Australia and expand the analyses to a longer observational record and a multicentury coupled climate model.

In contrast to the above studies whose focus is on the Indian Ocean, White (2000) found evidence that Australian precipitation covaries with Southern Ocean SST. He suggested that the tropospheric moisture flux convergence (divergence) varies such that anomalously moist (dry) marine air is advected onto Australia in phase with warm (cool) SST anomalies to the south, which are linked to the eastward propagation of the Antarctic Circumpolar Wave (ACW). The White (2000) study is, however, based on overall Australian and Western Australian rainfall, so it is of interest to reassess these proposed linkages in the context of the limited domain of SWWA.

The rest of this paper is organized as follows. The observational data and methodologies used in our study are described in section 2. In section 3 we examine observations and reanalysis data with a view to identifying anomalies in climate parameters associated with extreme rainfall events in SWWA. In section 4 we reassess the connection between Indian Ocean climate

and SWWA rainfall in a 1000-yr integration of a coupled climate model. In section 5 we briefly consider the seasonal evolution of the SWWA climate anomalies in both the model and observations. Finally, in section 6, we discuss and summarize our findings.

2. Observational data and data analysis

This study concentrates on southwest Western Australia in a region bound by 30°–35°S, 115°–120°E. To justify the localized region of analysis, Fig. 1a shows the net annual rainfall rate over the Australian mainland and Tasmania. Apparent in the west is a localized region of high rainfall—up to 900 mm yr⁻¹—falling within our study domain. This high rainfall region is not only unusual in the context of extratropical Western Australia; it is also relatively unique over the Southern Hemisphere. For example, at comparable latitudes both southwestern Africa and the subtropical western region of South America are characterized by somewhat lower regional rainfall rates (~300 mm yr⁻¹), in spite of much more pronounced orographic features than SWWA. A likely reason for the unusually high net rainfall over SWWA is the anomalously warm SST over much of the tropical and subtropical eastern Indian Ocean (Gentili 1991). The warm waters in the eastern Indian Ocean are due in part to the Indonesian throughflow from the western Pacific, as well as the resultant poleward-flowing Leeuwin Current, the world's only subtropical poleward-flowing eastern boundary current.

Observed annual rainfall for SWWA within our region of interest is shown in Fig. 1b during the period 1970–2003, with a power spectral density (PSD) analysis of this time series shown in Fig. 1c. Observations are taken from the gridded Australian Bureau of Meteorology (BoM) rainfall datasets, averaged over 30°–35°S and 115°–120°E. The time series in Fig. 1b is detrended and the long-term mean of 520 mm yr⁻¹ is removed. The trend in rainfall removed during 1970–2003 is in fact virtually negligible, at only -0.0264 mm yr⁻¹ per annum. This equates to less than 1 mm yr⁻¹ net decline in annual rainfall over the study region during the 34-yr record, indicating that our analysis period largely postdates the documented twentieth-century decline in SWWA rainfall (e.g., see analyses in IOCI 2002). The PSD analysis shows peak variability at periods of ~2.4, 3.9, and 8 yr (Fig. 1c). The standard deviation of the detrended rainfall time series is 66 mm yr⁻¹; this value is used to define anomalously wet and dry years, as indicated in Fig. 1b. In particular, wet (dry) years correspond to those years with rainfall one standard deviation above (below) the long-term mean. In absolute

terms, this means wet years receive $>586 \text{ mm yr}^{-1}$ and dry years $<454 \text{ mm yr}^{-1}$ of rainfall, respectively. It is important to note that while highest rainfall over SWWA occurs during austral winter, the extreme years defined above do not correspond exclusively to dry and wet winters. For example, some of the dry years do not correspond to winters of particularly low rainfall, and in some cases high summer rainfall rates push the year average into a wet-year anomaly. With the focus of this paper on year-to-year and not seasonal variations, and with annual rainfall extremes not defined exclusively by wintertime rainfall rates, it is appropriate to form composite statistics based on net annual mean conditions. In section 5 we briefly examine the nature and evolution of subannual rainfall anomalies over SWWA.

As direct observations are sparse over the extratropical oceans, including the South Indian and Southern Oceans, we employ reanalysis data to investigate large-scale atmospheric properties during dry/wet years over SWWA. Only the period since 1970 is considered, as prior to this time open-ocean data coverage is extremely sparse. The reanalysis data used are that of the National Centers for Environmental Prediction (NCEP) and National Center for Atmospheric Research (NCAR) reanalysis project (Kalnay et al. 1996). It is presently the most extensive reanalysis record available. The NCEP–NCAR reanalyses use a global spectral model with a horizontal resolution of T62 ($\sim 2^\circ$ latitude by $\sim 2^\circ$ longitude) and 28 unequally spaced vertical sigma levels in the atmosphere (Kalnay et al. 1996). The model includes parameterizations of all major physical processes. A variety of in situ and satellite measurements are assimilated and subjected to quality control before incorporation into the model. For this study, the following NCEP–NCAR reanalysis variables will be discussed: air temperature, sea level pressure (SLP), wind vectors, moisture advection, and outgoing longwave radiation (OLR). For oceanic properties we use the National Oceanic and Atmospheric Administration (NOAA) extended reconstructed SST dataset with a resolution of $\sim 2^\circ$ latitude by $\sim 2^\circ$ longitude. The NOAA climatology employs the most recently available Comprehensive Ocean–Atmosphere Data Set (COADS) SST data and improved statistical methods allowing for stable reconstruction using sparse data.

To investigate teleconnections to rainfall variability over larger scales we use the Climate Prediction Center (CPC) Merged Analysis of Precipitation (CMAP; Xie and Arkin 1996) climatology. The CMAP dataset is used instead of the NCEP–NCAR reanalysis rainfall, as potential deficiencies on regional scales were revealed in the latter by Janowiak et al. (1998) for parts of the

Indian Ocean and over Indonesia.¹ The CMAP dataset consists of monthly averaged precipitation on a $\sim 2.5^\circ$ latitude by $\sim 2.5^\circ$ longitude grid for the period 1979–2003. It combines several datasets of varying origin and characteristics, including gauge-based analyses from the Global Precipitation Climatology Center, predictions by the operational forecast model of the European Centre for Medium-Range Weather Forecasts, and three types of satellite estimates. As a further assessment of our findings obtained using the various climatological datasets, we will also examine SWWA rainfall variability within a multicentury integration of a coupled climate model (described in section 4).

To form composites of anomalous fields for a variety of parameters during dry and wet years, anomalies were calculated as the deviation of the composite annual mean from the long-term annual mean. By analyzing composite properties, prominent features of selected years are enhanced, while noise present in individual events is mostly removed. Dry SWWA years comprise 1972, 1977, 1979, 1987, 1994, and 2002, while wet SWWA years are 1973, 1974, 1988, 1992, and 1999 (for further details see Fig. 1b). For reference, years identified by Saji et al. (1999) as Indian Ocean Dipole years for the period 1970–99 are the following: 1972, 1982, 1994, and 1997, as is also indicated in Fig. 1b. Thus, it is noted that not all IOD events force anomalously dry conditions over southwest Western Australia, and indeed some dry years occur in the absence of an anomalously positive IOD phase.

3. Observed climate during extreme years

a. Rainfall

Composite analyses of annual surface precipitation rate show distinctly different patterns for dry (Fig. 2a) and wet (Fig. 2b) years in SWWA. The composite maps in Fig. 2 use rainfall rates from the CMAP climatologies binned into dry and wet years. It should be noted that Fig. 2 shows the raw composite rainfall anomalies, which tend to be large where the mean annual precipitation is highest (e.g., over Southeast Asia). While rainfall anomalies over SWWA do not appear large, mean precipitation there is relatively low compared to the Tropics, so the normalized anomalies at SWWA are significant. Anomalously low (high) rainfall persists over much of Southeast Asia and the tropical eastern

¹ It is noted that the composite rainfall maps in Fig. 2 are nonetheless relatively insensitive to the choice of rainfall climatology, including the CMAP, NCEP–NCAR, and Global Precipitation Climatology Project (GPCP) datasets.

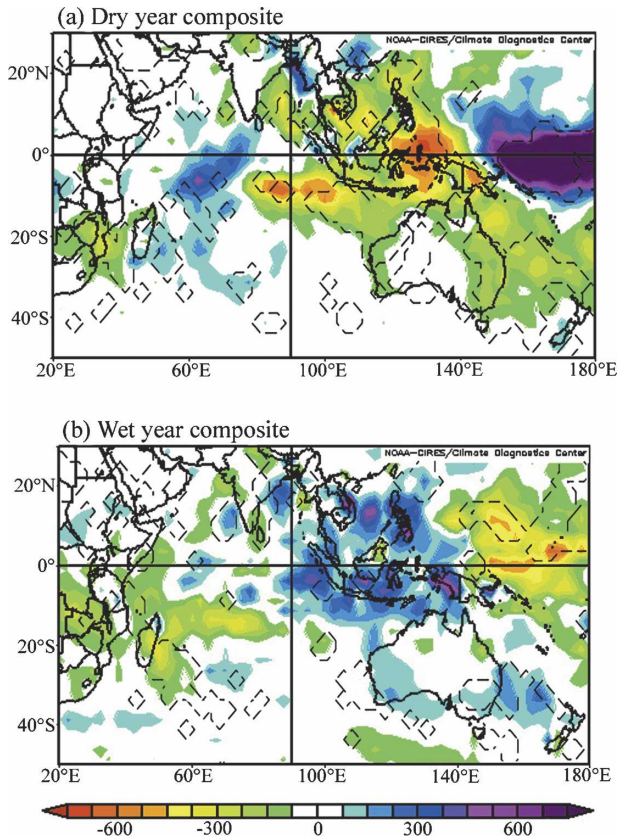


FIG. 2. Composite of anomalous CMAP surface precipitation rate (mm yr^{-1}) for (a) dry and (b) wet years in SWWA, as compared to the long-term climatological mean. Note that only extreme years from 1979 to 2003 are used to form the composites, as the CMAP rainfall climatology is only available from 1979. The dashed contours indicate where anomalies exceed the 90% significance level as estimated by a two-tailed t test.

Indian Ocean during dry (wet) SWWA years (Fig. 2). Dry (wet) years in SWWA appear to also coincide with dry (wet) years along Australia's eastern seaboard and wet (dry) years in the tropical western Pacific and western Indian Oceans. Hence, dry and wet conditions in southwest Western Australia appear to be part of a large-scale phenomenon affecting the Indian Ocean Basin and adjacent regions, in particular Southeast Asia, parts of East Africa, and eastern Australia.

b. Sea level pressure

Composite anomalies of SLP fields show that during dry years SLP over the Australian continent is unusually high (up to 1 mb above the long-term mean) with its center over southern Australia (Fig. 3a). A band of anomalously low pressure sits farther south so that geostrophic wind anomalies drive an intensified westerly wind field at 40°S. The pattern for wet years in SWWA

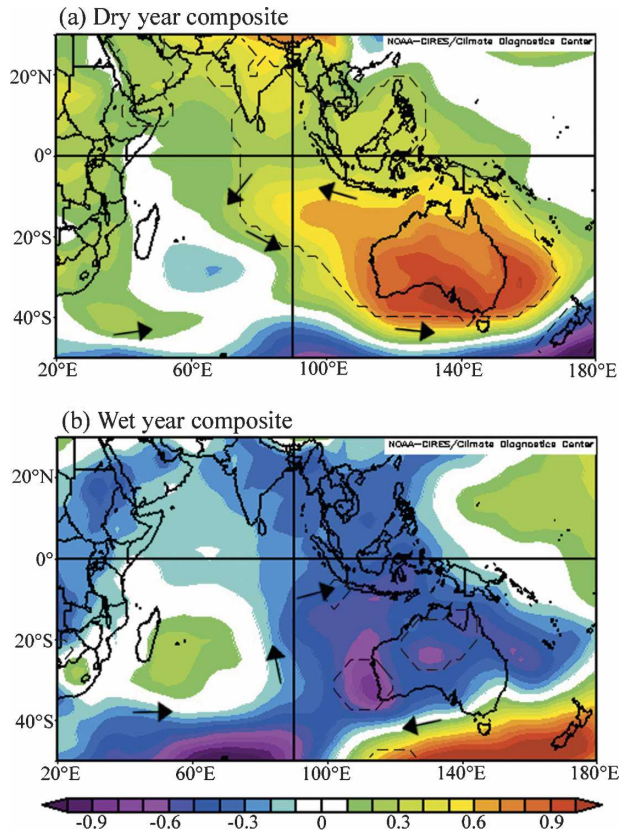


FIG. 3. NCEP-NCAR reanalysis composite of anomalous SLP (mb) for (a) dry and (b) wet years in SWWA, as compared to the long-term climatological mean. Overlaid on the diagrams are several vectors showing the direction of anomalous geostrophic winds during dry and wet years. The dashed contours indicate where anomalies exceed the 90% significance level as estimated by a two-tailed t test.

(Fig. 3b) is more or less reversed. However, in wet years, the anomalous low SLP across Australia and the eastern Indian Ocean stretches southward to the subpolar region near 60°E. A band of higher-than-normal SLP appears to the south of Australia, corresponding to weaker geostrophic westerly winds at 100°–140°E. With the wet and dry year composites exhibiting significant SLP anomalies over southern Australia and the Southern Ocean, the SWWA rainfall extremes could be related to the ACW or the Southern Annular Mode. However, analyses of time-lagged SLP maps (figures not shown) reveal little signal of an ACW leading up to wet/dry years, and the SLP anomaly patterns are not circumpolar, so neither of these scenarios appears likely.

c. Surface winds

The pressure anomalies, in turn, result in changed surface wind fields across wide parts of the Southern

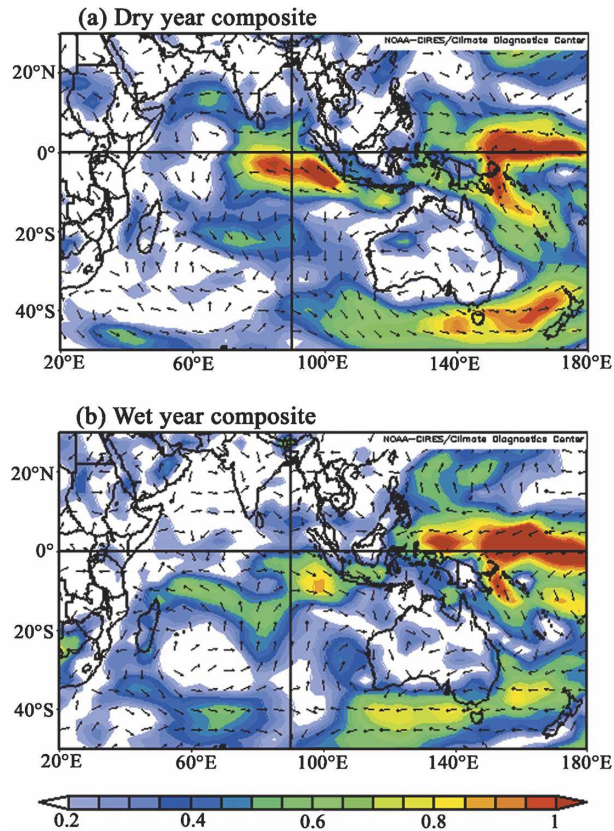


FIG. 4. Same as in Fig. 3, but for annual surface wind vector direction and speed (m s^{-1}). Vectors indicate direction only, with color shading denoting speed in m s^{-1} . Wind anomalies in excess of 0.5 m s^{-1} are significant at the 90% confidence level, as estimated by a two-tailed t test.

Hemisphere, as the winds closely track the pressure fields as expected under geostrophy (composite wind anomalies are shown in Fig. 4). This is especially apparent in the subpolar westerlies to the south of the Australian continent, which are strengthened (weakened) by the increased (decreased) meridional SLP gradient during dry (wet) years. A strengthening and coinciding southward shift of the subpolar westerlies to the south of Australia during dry years results in a similar southward shift of the rain-bearing fronts associated with the subpolar front. This situation is reversed during wet years, confirmed by composite plots of moisture advection in the region (figure not shown). Nearer the region of SWWA, Fig. 4 shows that the local surface winds are anomalously offshore during dry years and onshore during wet years. These localized wind changes have the effect of advecting less (more) moist air onto the west Australian coast during dry (wet) years (moisture advection figure not shown).

The composites of surface vector wind anomalies for dry and wet SWWA years also differ distinctly over the

Indian Ocean basin. For example, during dry (wet) years there is a strengthening (weakening) of the easterly winds on the northern flank (0° – 10°S , 70° – 110°E) of the gyre-scale anticlockwise wind system (Fig. 4). This agrees with the high (low) SLP anomaly extending from Australia northward across Southeast Asia. This extension of the SLP anomaly creates a divergence (convergence) in near-surface flow across Indonesia, resulting in subsidence (convection) of upper-atmospheric air masses, which leads to reduced (increased) local precipitation. Accordingly, decreased (increased) cloud formation is observed in the anomalous patterns of OLR (figure not shown) across Southeast Asia and SWWA (increased OLR for clearer skies, decreased OLR for greater cloud coverage). These mechanisms explain the pattern of anomalous rainfall (Fig. 2) seen across Southeast Asia during dry and wet years in SWWA. Additionally, there is a broad band of anomalous meridional winds at 15° – 30°S and 80° – 110°E during extreme SWWA rainfall years; characterized by unusually strong southward (northward) components during dry (wet) years. We will see below that these north–south wind anomalies contribute to local changes in atmospheric and oceanic temperatures. In summary, annual rainfall extremes over SWWA coincide with anomalies on both the tropical and extratropical flanks of the gyre-scale anticlockwise Indian Ocean wind system, with additional midbasin meridional wind anomalies occurring near $\sim 100^{\circ}\text{E}$.

d. Sea surface and air temperature

Anomalous SST composite maps for extreme SWWA rainfall years are shown in Fig. 5. In the eastern Indian Ocean a prominent dipole in SST exists off Western Australia during years of extreme rainfall; one pole (P1) is centered over the Northwest Shelf extending northwestward to Sumatra, and the other pole (P2) sits over the open ocean to the southwest centered at $\sim 30^{\circ}\text{S}$, 100°E . A third local extreme (P3) in SST is also apparent in the southwest Indian Ocean to the southeast of southern Africa.

The SST pole south of Indonesia (P1) can be explained by the anomalous wind fields of Fig. 4. During dry years, strong easterly wind anomalies (Fig. 4a) cause a shoaling of the thermocline (forced by increased Ekman transport away from the equator), resulting in anomalously cold upwelled waters. The opposite occurs during wet years (Fig. 4b), with weaker easterly winds allowing local SST to warm via reduced upwelling. During dry years, a warm pole in SST is also seen in the equatorial western Indian Ocean off Africa reminiscent of the IOD, likely a result of anomalous eastward advection of warm tropical waters originating

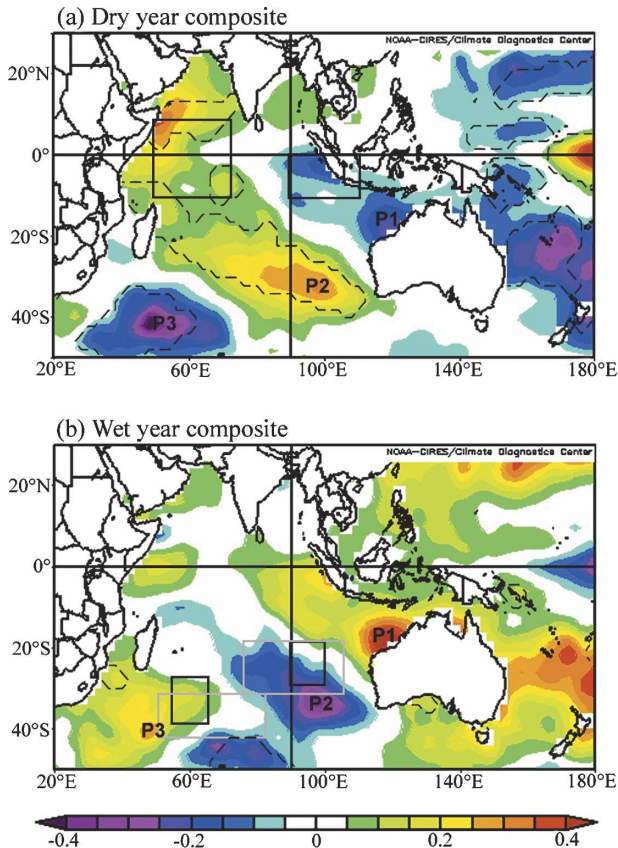


FIG. 5. Composites of anomalous annual NOAA extended reconstructed SST ($^{\circ}\text{C}$) for (a) dry and (b) wet years in SWWA, as compared to the long-term climatological mean. The areas traditionally associated with the IOD (Saji et al. 1999) and the SIOD (Behera and Yamagata 2001, solid boxes; Suzuki et al. 2004, gray boxes) are marked in (a) and (b), respectively. Labeled in each panel is the location of the temperature poles P1, P2, and P3 as discussed in the text. The dashed contours indicate where anomalies exceed the 90% significance level as estimated by a two-tailed t test.

from the eastern Indian Ocean. This results in a positive air–sea feedback of anomalous SST fields reinforcing the overlying anomalous winds. A signature of negative IOD phase is, however, only marginally apparent in the composite analysis of wet SWWA years (as noted below, only some wet years coincide with a strongly negative phase of the IOD).

The temperature pole located in the southeast Indian Ocean (P2; near 30°S , 100°E) corresponds with the anomalous meridional wind fields discussed in section 3c. For example, during dry years (Fig. 5a), the warm SST pole coincides with anomalous winds from the north (in fact, except for 2002, individual years show either anomalously weak southerly winds, or indeed, a mean northerly wind stream at this location). In contrast during wet years, the cold SST pole coincides with

enhanced southerly winds. This suggests that this second pole in SST is forced by local air–sea heat fluxes (unlike the tropical pole that appears to be the result of anomalies in wind-driven ocean advection). This is confirmed by composite analyses of observed air–sea heat fluxes (figure not shown), which show enhanced ocean heat loss over pole P2 during wet years (cool SST), and weakened ocean heat loss at pole P2 during dry years (warm SST). The air–sea coupling at P2 is apparent in the composite analyses of surface air temperature (Fig. 6), which show a prominent anomaly in heat content of the air mass overlying the southeast Indian Ocean SST pole. This confirms that the second SST pole is associated with anomalous warming (dry years) and cooling (wet years) forced by air–sea heat fluxes via meridional wind anomalies.

The third SST pole in Fig. 5 lies in the southwest Indian Ocean off southern Africa (P3). The SST anomalies in this region may be explained by anomalous wind-driven ocean advection during dry years (the cool water there is consistent with a stronger Ekman transport from the south), and anomalous air–sea heat

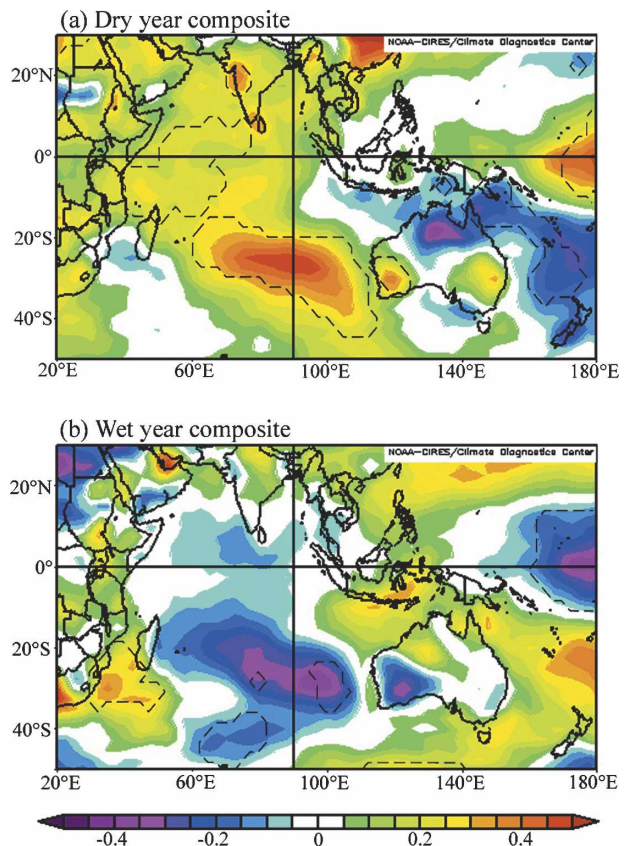


FIG. 6. Same as in Fig. 3, but for surface air temperature ($^{\circ}\text{C}$). The dashed contours indicate where anomalies exceed the 90% significance level as estimated by a two-tailed t test.

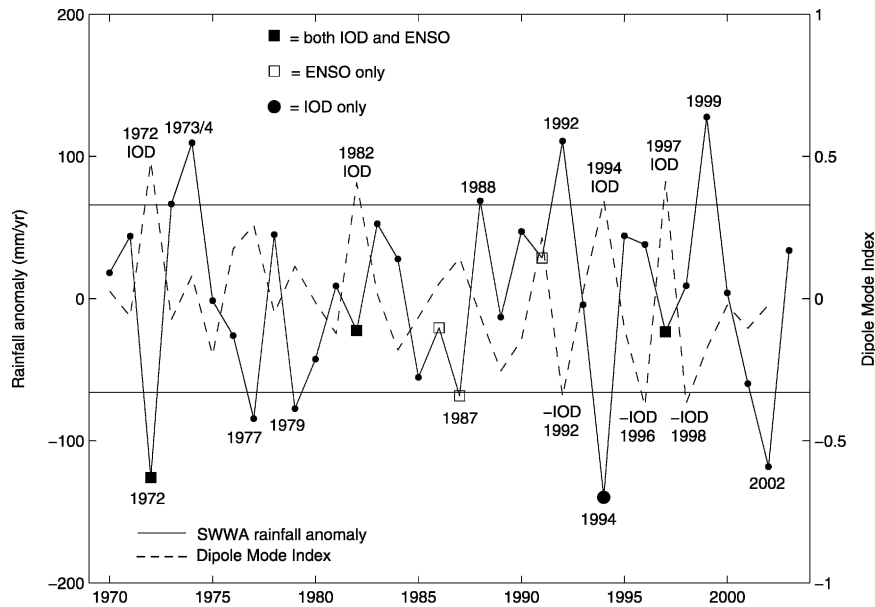


FIG. 7. Observed annual rainfall anomaly (solid line, mm yr^{-1}) for SWWA during 1970–2003 overlaid with the annual mean Indian Ocean DMI [dashed line, as defined by Saji et al. (1999)]. The Indian Ocean DMI is calculated using the regions indicated in Fig. 5a and the NOAA extended reconstructed SST climatology. Years identified as IOD years and ENSO years are indicated (\blacksquare = both IOD and ENSO; \square = ENSO only; \bullet = IOD only). ENSO year definitions are taken from MEY. Years of significant negative IOD phase are also indicated. The criteria used for wet/dry SWWA years are included (i.e., one standard deviation above/below the mean).

fluxes during wet years (an anomalous northerly air stream flows toward P3 in the wet-year composite).

It is finally worth noting that the SST composite signatures shown in Fig. 5 bear some similarity to previous analyses of surface temperature patterns in the Indian Ocean. For example, Nicholls (1989) found a significant correlation between northwest Western Australian (NWWA) winter rainfall and a pattern of SST reminiscent of poles P1 and P2 in our analysis. Surprisingly, Nicholls (1989) found no significant connection between his SST dipole and SWWA rainfall. Instead, his SST dipole was shown to correlate to rainfall over a region stretching from NWWA through central Australia and down to the southeast of the continent (matching the approximate trajectory of a northwest cloud band originating off NWWA). Ansell et al. (2000a) found that a similar SST dipole to Nicholls (1989) was correlated to Victorian rainfall in the southeast of Australia. More recently, Saji and Yamagata (2003b, their Fig. 2) plotted a composite map of the Indian Ocean SST anomaly during September–November based on seven of the coolest SST anomaly years at 7°S , 105°E , which sits over the eastern pole of the IOD (to the northwest of P1). While the resulting SST composite shows only a weak cool signature at our pole P1, it

reveals a warm band of SST spanning from the western pole of the IOD off Africa southeastward toward SWWA (reminiscent of the pattern of SST seen in our Fig. 5a). This correspondence reflects the IOD component in our composite dry year analysis for SWWA rainfall.

e. Relation to the IOD and SIOD

It has already been mentioned that in some years the Indian Ocean dipole is associated with SWWA rainfall via the reinforcement of SST anomalies at pole P1. The IOD may also affect SWWA rainfall by other means, such as via a modification of the tropical wind field as is suggested by the anomalies seen in Fig. 4. To investigate the IOD–SWWA rainfall link further we calculate the Indian Ocean dipole mode index (DMI), an indication of IOD strength, and plot its annual mean against SWWA rainfall anomalies in Fig. 7. All properties shown in Fig. 7 represent the annual mean of monthly values. In particular, we calculate the monthly DMI using monthly SST values before forming the annual mean. The DMI definition is as described by Saji et al. (1999); namely, the difference is taken between spatially averaged NOAA reconstructed SST anomalies of two areas in the Indian Ocean (shown in Fig. 5a),

one in the western Indian Ocean (10°S–10°N, 50°–70°E) and the other in the tropical eastern Indian Ocean (0°–10°S, 90°–110°E). In the DMI, the eastern SST anomaly is subtracted from the western SST anomaly.

The most obvious aspect of Fig. 7 is that the DMI and SWWA rainfall are strongly out of phase. However, not all IOD events force anomalously dry conditions over southwest Western Australia, and indeed some dry years occur in the absence of an anomalously positive IOD phase. The DMI is correlated negatively with rainfall in SWWA, with a Pearson correlation coefficient of -0.534 and an associated P value of 0.001 . The connection between the IOD and SWWA rainfall is most apparent, however, during dry years, with the dry year SST composite anomaly pattern typical of an IOD event (Fig. 5a), yet only a weak signature of negative IOD phase during wet years (Fig. 5b). Nonetheless, several of the anomalous wet years coincide with a negative phase in the DMI, most notably 1992 (Fig. 7). During such years the IOD acts to strengthen the SST anomalies south of Indonesia as well as enhancing wind anomalies along the northern flank of the Indian Ocean anticyclone, thereby affecting the mean subtropical ridge that drives winds and moisture onto the coast of SWWA.

The combination of SST anomalies at P2 and P3 is reminiscent of the subtropical Indian Ocean Dipole (SIOD), although as indicated in Fig. 5 the location of these anomalies does not match previous definitions of the SIOD. For example, Suzuki et al. (2004) investigate a subtropical dipole of SST at 42°–30°S, 50°–80°E, (southwestern pole) and 29°–17°S, 75°–105°E (northeastern pole). Neither of these two poles overlies the regions of high SST anomaly identified above. It is not surprising then, that the subtropical dipole index (SDI) of Suzuki et al. (2004) is not significantly correlated with SWWA rainfall (Pearson correlation coefficient of 0.238 , and an associated P value of 0.183). Similar correlation levels are obtained between SWWA rainfall and the SDI of Behera and Yamagata (2001). We further investigated time series of the seasonal mean SDI indices versus seasonal mean SWWA rainfall and again found no significant correlation.

In spite of this, it is clear that extremes in SWWA rainfall are associated with subtropical and midlatitude Indian Ocean SST and SLP anomalies, which in turn modulate the subtropical high and thereby alter the local atmospheric circulation (Figs. 3, 4). In the context of our study region, SWWA rainfall extremes are related to subtropical SST anomalies at locations to the east of previous definitions of the SIOD (e.g., as depicted in Fig. 5). This is supported by the magnitude of

anomalous winds in the southwest Indian Ocean shown in Fig. 4, which are weaker than those in the east, particularly during dry years. Anomalies in the southwest Indian Ocean (near P3) are thus likely symptomatic of other basin-scale adjustments in the Indian Ocean anticyclone during dry and wet years and are not essential to the control of SWWA rainfall.

f. Modulation by ENSO

The focus of this paper is on the link between inter-annual SWWA rainfall variability and climate over the Indian Ocean. However, it is of interest to assess whether the link to Indian Ocean climate variability is in some way modulated by ENSO. Figure 7 highlights years during the 1970–2003 observational record that can be identified as IOD years, those identified as ENSO years [using the definition of Meyers et al. (2006, hereafter MEY)], and those identified as both IOD and ENSO years. For comparison the annual rainfall anomaly for SWWA is included in Fig. 7, and years of significant negative IOD phase are also shown. SWWA rainfall extremes exhibit no obvious link to ENSO events. For example, when an ENSO event occurs in the absence of a strongly positive IOD phase (1986, 1987, and 1991), SWWA rainfall is not significantly different to the long-term mean. Rainfall can be anomalously low during combined ENSO–IOD years (e.g., 1972), but it can also be average in such years (1982 and 1997). It is true that ENSO events tend to be associated with drier SWWA years, although the connection is by no means robust and could just be symptomatic of the known ENSO–IOD connection (e.g., just over 40% of IOD events during 1876–1999 have coincided with ENSO events; MEY). The teleconnection of ENSO to the IOD remains a topic of vigorous debate, and separating their projection onto SWWA rainfall is beyond the scope of the present study. Nonetheless, it is possible that ENSO directly plays a role in SWWA rainfall, for example, via a continent-wide SLP response through the downward branch of the Walker circulation.

4. Modeled climate during extreme years

One of the limitations of the above analyses of the observed and reanalysis records is that there are only 5–6 yr characterized by anomalously high or low SWWA rainfall (Fig. 1b). This means that in general, only the high-amplitude signatures of the observed composite analyses are statistically significant (e.g., the SST poles, the SLP anomalies over Australia, and the tropical and extratropical wind anomalies). A much

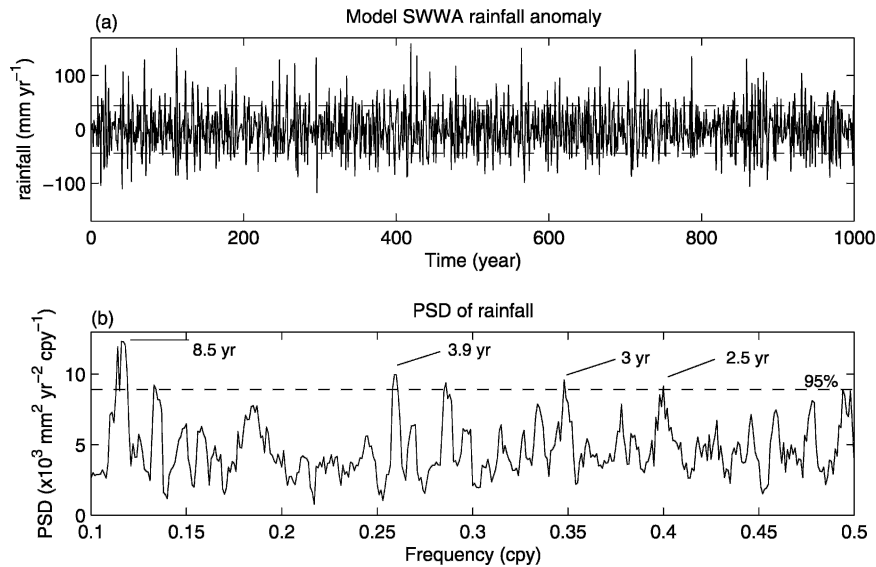


FIG. 8. (a) Time series of annual precipitation anomaly (mm yr^{-1}) in SWWA over the 1000-yr climate model simulation. The dashed lines indicate one standard deviation (44 mm yr^{-1}) above and below the 1000-yr mean, which is used to define anomalously dry and wet years. The model SWWA precipitation is defined as the average over the area indicated by the box at $30^{\circ}\text{--}35^{\circ}\text{S}$, $115^{\circ}\text{--}120^{\circ}\text{E}$ (see Figs. 9a,b for the location). (b) PSD of SWWA precipitation. The dashed line represents the estimated white noise spectrum at the 95% confidence level.

longer observational record is required to obtain detailed statistically significant patterns of Indian Ocean climate during wet and dry years over SWWA. It is therefore useful to revisit our analyses in the context of a long-term multicentury natural simulation of the global coupled climate system. To this end we examine 1000 yr of model data from the latter stages of a 10 000-yr integration of the Commonwealth Scientific and Industrial Research Organisation (CSIRO) coupled climate model under constant CO_2 forcing. The model used is an updated version of the climate simulation described by Hirst et al. (2000), consisting of coupled atmospheric, oceanic, sea ice, and land surface submodels. All components of the model have a horizontal spectral resolution of R21 (approximately 3.2° latitude \times 5.6° longitude), while on the vertical scale the ocean general circulation model (GCM) has 21 geopotential levels and the atmospheric GCM 9 sigma levels. The climate model employs seasonally varying heat and freshwater flux adjustment terms to keep the simulation near to a present-day steady state. Further details on the model physics and numerics, as well as its ability to simulate the present-day global climate, can be found in Gordon and O'Farrell (1997) and Hirst et al. (2000). Details of the model's representation of global climate variability and precipitation can be found in Walland et al. (2000) and Hunt (2001).

Since the focus of this study is on rainfall variability

on interannual time scales, a high-pass filter is applied to the model data to retain signals with periods of 2–10 yr. The model variables analyzed here include the annual mean SWWA rainfall (shown as a time series over 1000 yr in Fig. 8a, using rainfall averaged over the area indicated in Figs. 9a,b), as well as global SST, rainfall, surface wind stress, air–sea heat fluxes, and surface ocean currents. The SWWA rainfall shown in Fig. 8a is calculated using linear interpolation involving a total of 12 model grid points that span the domain of interest, matching the nearest model grid boxes to the analyzed observational domain of $30^{\circ}\text{--}35^{\circ}\text{S}$, $115^{\circ}\text{--}120^{\circ}\text{E}$. There are only 2 model grid points wholly enclosed by the box shown in Figs. 9a and 9b, but another 10 points adjacent to the region that come into the calculation of SWWA rainfall via an area-weighted linear interpolation.

The coupled climate model SWWA rainfall variability is weaker than that seen in the BoM observations, with a standard deviation of 44 mm yr^{-1} compared to the observed 66 mm yr^{-1} . This is typical of coarse-resolution climate models wherein extreme events tend to be weakly damped compared to observations. The extremes in model SWWA rainfall (Fig. 8a) are defined as those in which the rainfall anomaly exceeds one standard deviation above and below the long-term mean (i.e., $\pm 44 \text{ mm yr}^{-1}$), resulting in ~ 150 instances of each of anomalously wet and dry years. The dominant periods of interannual variability of the model SWWA rain-

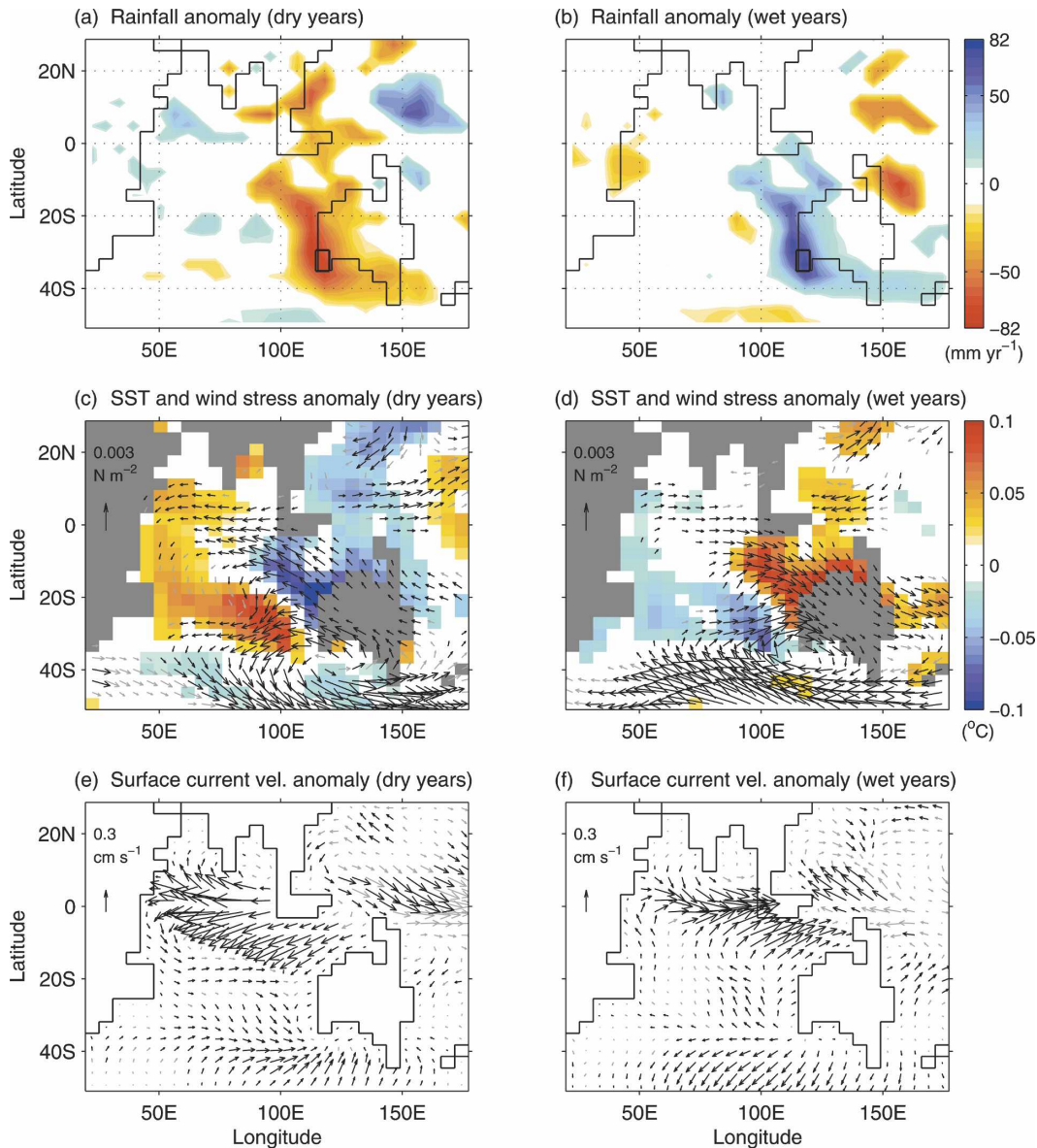


FIG. 9. Composite maps of (a), (b) rainfall anomaly, (c), (d) SST overlaid on vectors of wind stress anomaly, and (e), (f) ocean surface current anomaly during (a), (c), (e) dry and (b), (d), (f) wet years in the climate model. Anomalies are only shown where they exceed the 90% significance level as estimated by a two-tailed t test. Anomalous wind stress and surface current velocities below the significance level are displayed as gray vectors in (c)–(f). Wind anomaly vectors of magnitude less than $0.5 \times 10^{-3} \text{ N m}^{-2}$ are not shown. The highlighted box in (a)–(b) marks the SWWA location used to define years of anomalous model rainfall (i.e., the dry and wet years of Fig. 8a).

fall appear similar to the observations from a cursory comparison of Figs. 1b and 8a, which is confirmed by power spectral density analyses (Figs. 1c, 8b). The dominant variability in the model rainfall occurs at a broad range of periods, including 3–4 yr and ~ 8.5 yr (these peaks are significantly different at the 95% confidence level from a white noise signal; see Fig. 8b). The PSD analysis of observed rainfall (Fig. 1c) shows much less

structure than the model (to be expected given the short data record), although the observed peaks at 2.4, 3.9, and 8 yr are in good agreement with three of the significant peaks shown in the model analysis. The dominant period of variability seen in the observed SWWA rainfall (~ 4 yr; Fig. 1c) contrasts multiple significant peaks in the model (at $\sim 2.5, 3, 3.5, 4, 7,$ and 8.5 yr). It also contrasts the variability of the model's IOD,

which exhibits a dominant period of ~ 3 yr (figure not shown). The model IOD variability also exhibits a signal with a period of ~ 2 yr, although not of magnitude significantly different from background noise. Damped higher-frequency climate variability is a problem common to coarse-resolution models; it is likely to be why the simulation does not capture the primary biennial peak in the IOD noted in observations (e.g., Ashok et al. 2003a).

Composite anomalies of the model regional rainfall patterns during dry and wet SWWA years are shown in Figs. 9a,b. Anomalies are only shown where they exceed the 90% significance level as estimated by a two-tailed t test. The composite patterns of model precipitation correspond closely to those formed based on the observed 1979–2003 CMAP climatology (Fig. 2), though with reduced amplitude. Anomalous rainfall extends from SWWA and the eastern Indian Ocean into Asia in both dry and wet years, with a general reversal of sign over the western Indian Ocean and Africa, as well as in the western Pacific. Unlike the observed, however, the composite patterns exhibit highest anomaly magnitudes over SWWA, not Asia. This indicates a greater variety of rainfall scenarios over Asia in the model during dry and wet SWWA years. It is also noted that the model underrepresents tropical ocean–atmosphere variability, including ENSO and the IOD, owing to its coarse resolution and possibly the use of flux adjustment terms. In this context we repeated the model composite analyses within the nonflux-adjusted NCAR climate system model and found similar patterns to those described here (figures not shown).

Composites of the model SST and wind vector anomalies during dry and wet SWWA years are presented in Figs. 9c,d (as above, only shown where they exceed the 90% significance level). This shows that during dry years a pole of cold SST sits in the tropical eastern Indian Ocean off northwest Australia alongside a pole of anomalously warm SST to the south extending northeast toward central Africa. During wet years this SST pattern is reversed, with the dipole of temperature anomalies nearly a mirror image of the dry-year scenario. These dry- and wet-year patterns are remarkably similar to the reanalysis SST composite anomalies shown in Fig. 5, although the magnitude of the SST anomalies is smaller in the model compared to the observations ($\pm 0.1^\circ$ versus $\pm 0.4^\circ\text{C}$, respectively). This reduced SST variability is likely due to a combination of the model's coarse resolution, the model flux adjustment terms, and the fact that we composite ~ 150 model years for each of the low-rainfall and high-rainfall scenarios. Like the observational analyses (Fig. 5), the model SST dipole reaches peak amplitude in the tropi-

cal and subtropical eastern Indian Ocean, adjacent to Western Australia (and to the east of previous definitions of the subtropical Indian Ocean Dipole). Furthermore, the model composite of dry years shows a stronger magnitude IOD pattern compared to the model wet years, similar to the observed composite SST signals of Fig. 5.

The model composite winds are also for the most part consistent with the reanalysis data. There is a strengthening (weakening) of the subpolar westerlies during dry (wet) SWWA years (Figs. 9c,d). In addition, dry (wet) years are accompanied by acceleration (deceleration) of the tropical easterlies, with strongest anomalies off the Indonesian coast. As with the reanalysis data, this forces the oceanic heat anomalies at pole P1 via fluctuations in the surface Ekman transport away from the equator (this can be confirmed for the model in Figs. 9e,f). In addition, local evaporative fluxes also play a role in regulating the model's SST anomalies at P1. Winds over the southeast Indian Ocean SST pole (P2) include anomalously northward (southward) components during cold (warm) phases. These features again show excellent agreement between the reanalyzed and climate model data. As in the observed analyses, anomalies in the model air–sea heat exchange at pole P2 are controlling SST fluctuations via anomalous meridional winds (composite heat flux patterns not shown). Ocean advection also contributes to SST variability at P2, with meridional flow anomalies altering local ocean heat transport (Figs. 9e,f). The model wet (dry) years experience an increase (decrease) in onshore winds over southwest Western Australia near 30°S (Figs. 9c,d), which is also apparent albeit localized in the NCEP–NCAR data (Fig. 4). Anomalous ocean current fields (Figs. 9e,f) mostly reflect adjustments in Ekman transport as forced by the wind stress anomalies symptomatic of wet and dry years. These ocean circulation changes are important for forcing SST anomalies at pole P1 (via divergence of water from the equator) and in the extratropics under the subpolar westerlies.

5. Seasonal development of climate anomalies

The focus of this paper is on year-to-year precipitation anomalies over southwest Western Australia. Nonetheless, with the majority of SWWA rainfall occurring during austral winter (e.g., McBride and Nicholls 1983; Drosowsky 1993b), it is of interest to assess the intra-annual development of climate anomalies associated with extreme wet and dry years. Figure 10 shows the mean monthly precipitation over south-

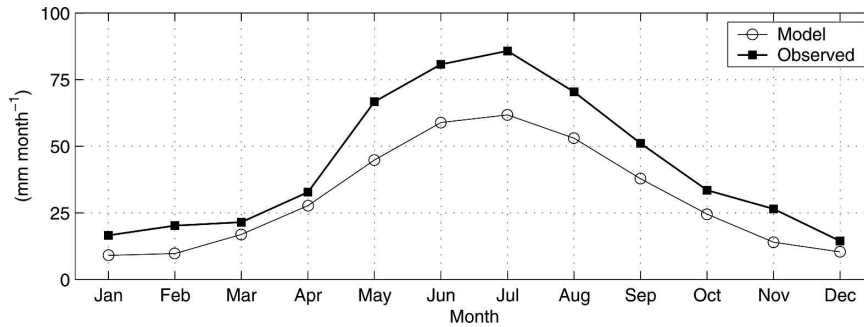


FIG. 10. Observed and modeled mean monthly precipitation over SWWA in mm month^{-1} . The observed is derived from the BoM gridded rainfall climatology during 1970–2003. The model seasonal cycle is derived from the CSIRO 1000-yr integration. The regions of analysis used to construct the observed and modeled means are shown in Figs. 1a and 9a, respectively.

west Western Australia during the 1000-yr model integration and during 1970–2003 in the observed. Both modeled and observed show peak rainfall occurring during June–July–August (JJA, hereafter 3-month periods are denoted by the first letter of each respective month), declining gradually to minimum rainfall during DJF. In both modeled and observed, approximately 45% of the total annual precipitation over SWWA occurs during JJA. To assess the seasonal development of climate anomalies associated with extreme wet and dry years, Fig. 11 shows the evolution of NCEP–NCAR sea level pressure anomalies during dry and wet years for the period 1970–2003. A corresponding analysis for NOAA extended reconstructed SST is presented in Fig. 12. In these analyses, the seasonal composites are formed using the extreme rainfall years to elucidate the seasonal evolution of annual climate anomalies, rather than looking at extremes of any given season in isolation (we undertake such an analysis for wintertime later in this section).

Figure 11 reveals that on average, extreme SWWA rainfall years are characterized by a progressive strengthening of anomalous SLP during the progression from summer to late winter months. This is not unexpected as peak rainfall occurs during austral winter, with DJF precipitation less than 25% of that received during JJA. In fact, summertime SLP anomalies in DJF (Figs. 11a,b) bear only weak resemblance to the peak wintertime pressure anomalies seen in Figs. 11e,f. Autumn (MAM), winter (JJA), and spring (SON) anomalies are all reminiscent of the annual patterns shown in Fig. 3. In contrast, sea surface temperature anomalies (Fig. 12) show greater persistence, with summertime SST patterns in DJF already exhibiting the characteristic three-pole structure noted in the annual composites (Fig. 5). The two areas of anomalous SST adjacent to SWWA (P1 and P2 of Fig. 5) reach peak magnitudes

in wintertime (JJA) and spring (SON), but their genesis appears as early as the preceding summer.

With our focus on interannual SWWA rainfall fluctuations, an analysis of extremes in seasonal precipitation is mostly beyond the scope of the study. We note, nonetheless, that composite analyses of seasonal rainfall extremes reveal similar Indian Ocean climate states to the wet and dry scenarios described in sections 3 and 4, particularly during April–November. For example, an analysis of extended wintertime (May–September) rainfall during 1970–2003 identifies six anomalously dry winters (1976, 1977, 1979, 1987, 2000, and 2002) and seven anomalously wet winters (1973, 1974, 1983, 1988, 1992, 1996, and 1999), using the ± 1 standard deviation criterion adopted previously. Figure 13 shows composite SLP, winds, and SST during the wet and dry winters identified above. The overall pattern of anomalous SLP and SST during extreme winters is very similar to the annual composite anomalies described previously, despite a different selection of years in the composite statistics. Some notable differences appear in the wind composites, which are now dominated by anomalous patterns of onshore and offshore winds at the latitude of SWWA. Overall, the peak in surface pressure anomalies appears to be shifted slightly to the south compared to the annual composites, with a weakened tropical influence on SWWA during wintertime. This is likely due to the increased role of extratropical cyclones during winter in feeding moisture to SWWA, as compared to other seasons when northwest cloud bands may dominate. Apart from these differences in composite winds, the overall patterns of SST and SLP characteristic of SWWA winter rainfall extremes exhibit strong similarity to the annual composites detailed in section 3. Thus, our results for the Indian Ocean climate states associated with *annual* SWWA rainfall extremes are robust when applied to an analysis of

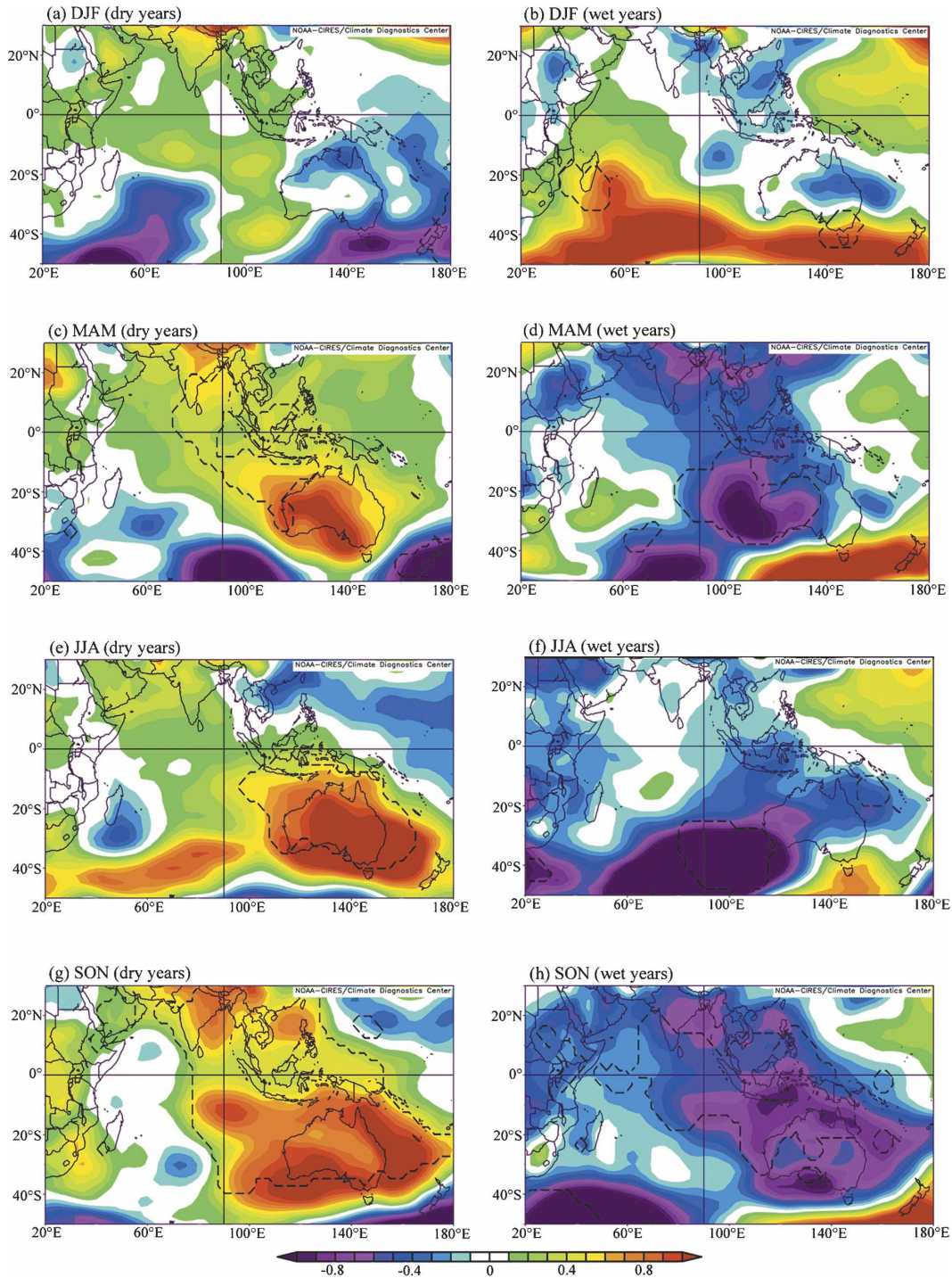


FIG. 11. Seasonal evolution of NCEP-NCAR reanalysis SLP anomalies (mb) for (left) dry and (right) wet SWWA years for the period 1970–2003, as compared to the long-term climatological seasonal mean. The dashed contours indicate where anomalies exceed the 90% significance level as estimated by a two-tailed t test.

SWWA *winter* rainfall extremes. While not shown here, analyses of SST, SLP, and winds during austral autumn (MAM) and spring (SON) extremes also exhibit robust features compared to those described for the annual

extremes. In contrast, composite analyses based on extreme summertime (DJF) rainfall events show robust patterns of SST, similar to the features revealed in Fig. 5, and largely robust patterns in SLP and winds during

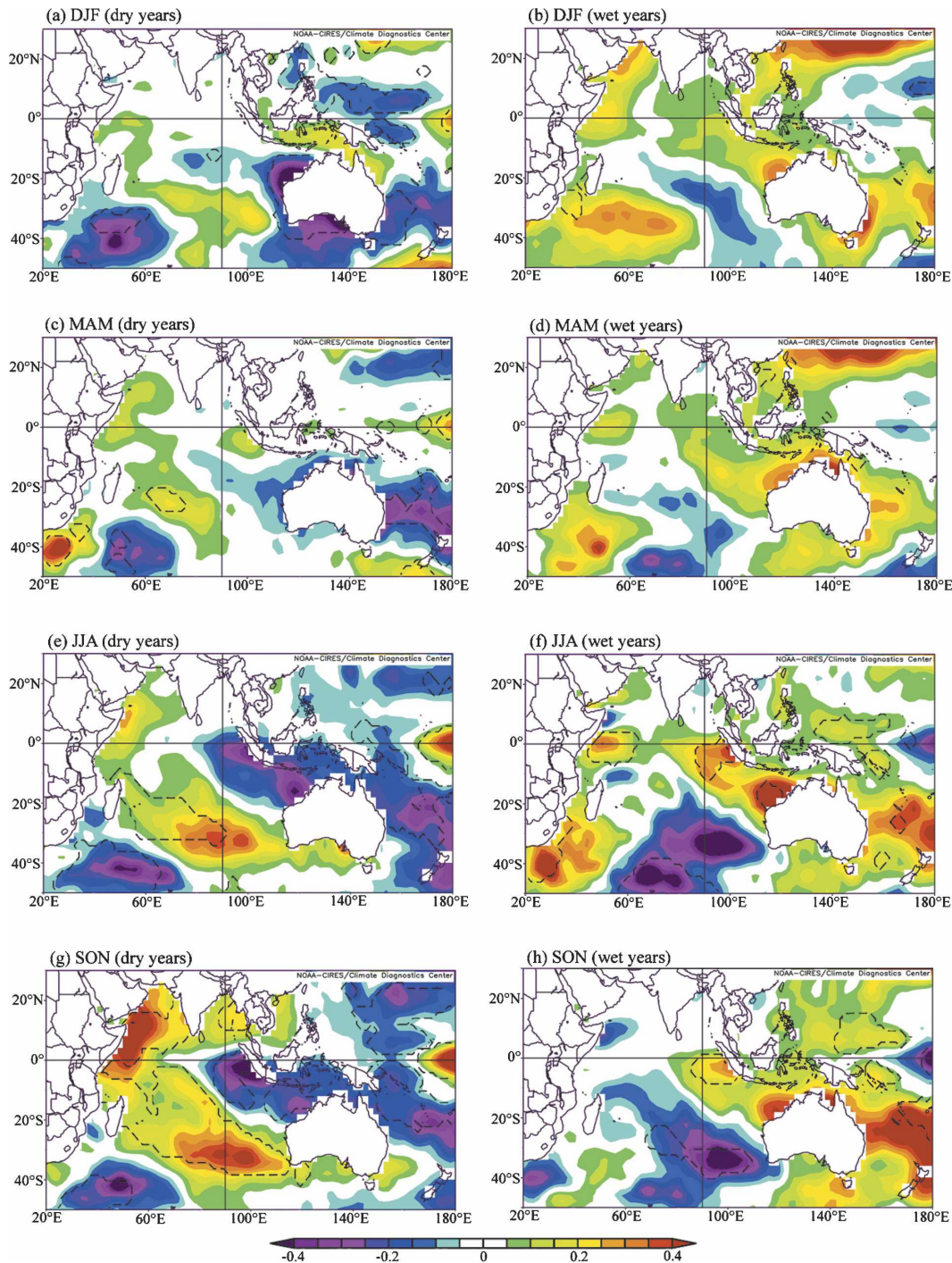


FIG. 12. Same as in Fig. 11, but for NOAA extended reconstructed SST anomalies ($^{\circ}\text{C}$).

dry summers, but significant differences in SLP and winds for anomalously wet summers (figure not shown).

An analysis of the climate model's seasonal evolution of SST and wind anomalies during wet and dry years is presented in Fig. 14. Like the evolution of climate

anomalies within observed wet/dry years (Figs. 11–12), the model exhibits a progressive amplification of anomalies in SST and atmospheric circulation toward a wintertime peak during JJA. The composite plots suggest that ocean temperature anomalies begin to develop as early as summertime, with a weak SST dipole

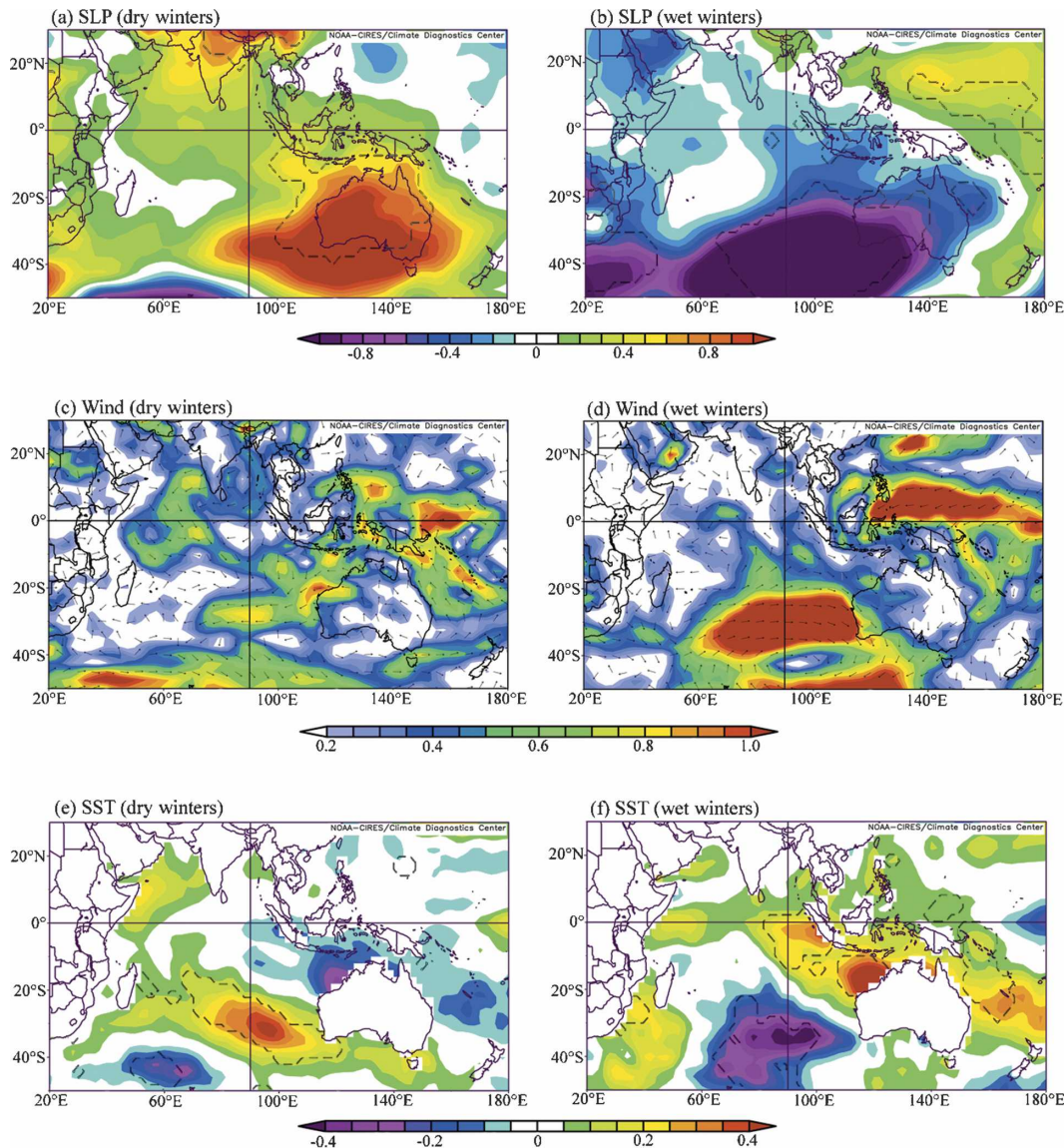


FIG. 13. Composite analyses of (a), (b) SLP (mb), (c), (d) vector winds (m s^{-1}), and (e), (f) SST ($^{\circ}\text{C}$) for (a), (c), (e) dry and (b), (d), (f) wet winters in SWWA. The extreme winter rainfall events are defined as one standard deviation below/above the mean rainfall during May–September (inclusive). Years included in the composite winter analysis are given in the text. The dashed contours indicate where anomalies exceed the 90% significance level as estimated by a two-tailed t test. Wind anomalies in excess of 0.5 m s^{-1} are significant at the 90% confidence level, as estimated by a two-tailed t test.

appearing at P1 and P2 in the mean DJF conditions. Wind anomalies then develop during the ensuing months (MAM), amplifying to a pronounced large-scale acceleration (deceleration) of the Indian Ocean mean anticyclone by wintertime (JJA) during dry (wet) years. The wind anomalies reinforce the SST anomalies via Ekman transport at P1 and air–sea fluxes at P2, yielding peak amplitude SST anomalies during JJA. The Indian Ocean climate anomalies then begin to weaken gradually during austral spring (SON). Thus in

summary, both the model and observed extreme years exhibit a seasonally evolving climate signal over the Indian Ocean, appearing to initiate in SST as early as summertime, rapidly increasing to a peak amplitude in atmospheric circulation and SST during winter, then abating gradually during austral spring.

6. Discussion and conclusions

We have assessed interannual rainfall extremes over southwest Western Australia using 34 yr of observa-

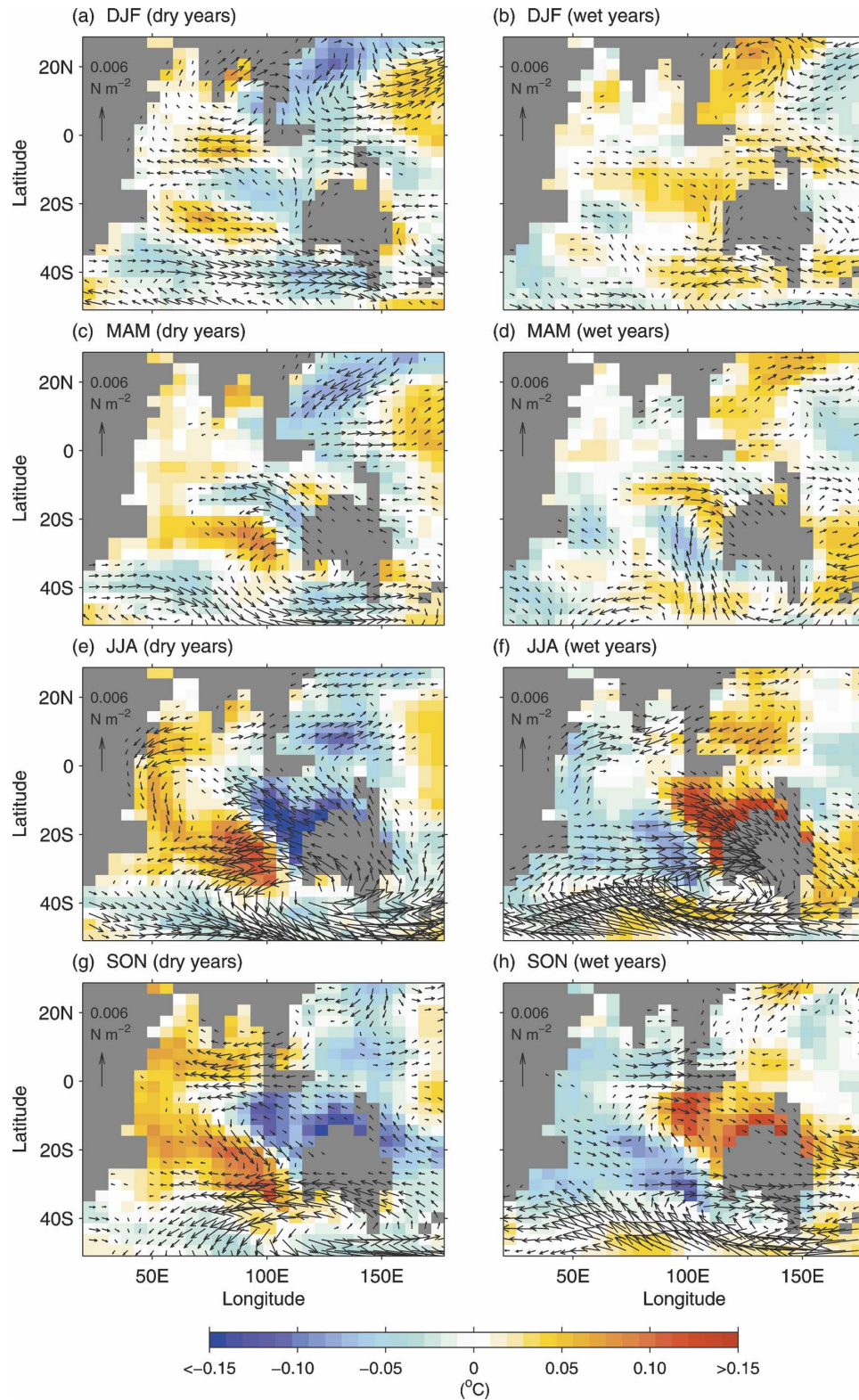


FIG. 14. Seasonal evolution of SST and wind stress anomalies presented as composite maps based on extreme years of SWWA rainfall in the coupled climate model: (left) dry and (right) wet years. Wind anomaly vectors of magnitude less than $0.5 \times 10^{-3} \text{ N m}^{-2}$ are not shown. Anomalies are only shown where they exceed the 90% significance level as estimated by a two-tailed t test.

tions and reanalysis data as well as 1000 yr of model output from a global coupled climate model integration. The study area is limited in its spatial extent but is chosen because of its unique rainfall characteristics, which are confirmed in this study to be of a highly localized nature. Both the reanalysis data and the climate model suggest SWWA rainfall extremes are linked to a reorganization of the large-scale wind field over the eastern and southeastern Indian Ocean. The wind field alters SST via anomalous Ekman transport in the tropical Indian Ocean and via anomalous air–sea heat fluxes in the subtropics, as well as changing the large-scale advection of moisture onto the SWWA coast. The resulting dipole in SST seesaws in sign between dry and wet years, and is different from most previous definitions of SST dipoles in the region. In particular, the dipole we linked to SWWA rainfall exhibits peak amplitudes in the eastern Indian Ocean adjacent to the west coast of Australia. During dry years, the SST pattern is characterized by anomalously cool waters in the tropical eastern Indian Ocean (P1; Fig. 5), adjacent to a region of unusually warm water in the subtropics off SWWA (P2). In some of the dry years, the cool temperatures in the tropical eastern Indian Ocean are reinforced by an Indian Ocean Dipole event. Notably, however, not all IOD events force anomalously dry conditions over southwest Western Australia, and indeed some dry years occur in the absence of an anomalously positive IOD phase (Fig. 7). In a similar manner, some (but not all) wet SWWA years are reinforced by a negative phase in the Indian Ocean Dipole.

The fact that there is no simple relationship between interannual variability in SWWA rainfall and the IOD suggests that other low-frequency processes are also at play. These include the modes of subtropical and extratropical variability that have already been described above. In addition, the proximity of the first SST pole (P1) to the Indonesian Archipelago suggests that variations in the Indonesian throughflow (ITF) will also drive substantial SST variability at P1. In addition, the Leeuwin Current propagates heat content anomalies from P1 poleward along the west coast of Western Australia, offshore of the SWWA region, and so it too likely impacts local wind and moisture advection anomalies in the region. These modes of variability cannot be examined using observational data, however, as direct ocean current measurements are too sparse. In addition, coupled climate model resolution is inadequate to resolve the structure and speed of the Leeuwin Current. Hence, we cannot easily assess the role of the ITF and Leeuwin Current variability in determining SWWA rainfall in the present study.

As noted above, anomalous winds during extreme years alter SST via Ekman transport in the tropical Indian Ocean and via air–sea heat fluxes in the subtropics. The winds also change the large-scale advection of moisture onto the SWWA coast. At the basin scale, the anomalous winds can be interpreted as an acceleration (deceleration) of the Indian Ocean climatological mean anticyclone during dry (wet) years. In addition, dry years see a strengthening and coinciding southward shift of the subpolar westerlies, which results in a similar southward shift of the rain-bearing fronts associated with the subpolar front. A link is also noted between extreme rainfall years and winds over the tropical margin of the Indian Ocean anticyclonic, which reinforces the tropical eastern pole of SST described above. In this manner, both tropical and extratropical processes in the Indian Ocean generate SST and wind anomalies off western Australia, which are linked to moisture transport and rainfall extremes in the region.

A schematic diagram depicting the major climate anomalies during dry and wet years over SWWA is shown in Fig. 15. During dry years, a strengthening of the northern flank of the anticyclonic wind field across the equatorial Indian Ocean causes a shoaling of the thermocline and cool upwelled SST off the Indonesian coast, accounting for the simultaneously dry conditions in Southeast Asia. This is sometimes reinforced by an Indian Ocean Dipole event. The cool SST anomalies exhibit highest magnitude adjacent to the west Australian coast (P1 of Fig. 5). In addition, dry years coincide with an anomalous southward air stream over the eastern subtropical Indian Ocean, leading to warmer air, anomalous air–sea heat fluxes, and warmer SST centered near 30°S and 100°E (pole P2 of Fig. 5). Farther south, the dry-year climate exhibits a strengthening and coinciding southward shift of the subpolar westerlies, which results in a similar southward shift of the rain-bearing fronts associated with the subpolar front. This leads to reduced moisture transport onto the SWWA region. The dry year climate dynamics are more or less reversed during wet years, although only a weak IOD signal is noted in the composite analyses. During wet years, anomalously low air pressure extends over much of the region, driving a deceleration of the Indian Ocean subtropical anticyclone. In the immediate vicinity of SWWA, winds are anomalously stronger onshore, forcing increased moisture transport into the region.

A 1000-yr integration of a coupled climate model was used to reassess the results of the 34-yr reanalysis record, particularly in view of the low number of extreme events available in the short observational record. Analysis of the ~150 extreme dry and wet SWWA years in the climate model simulation revealed surpris-

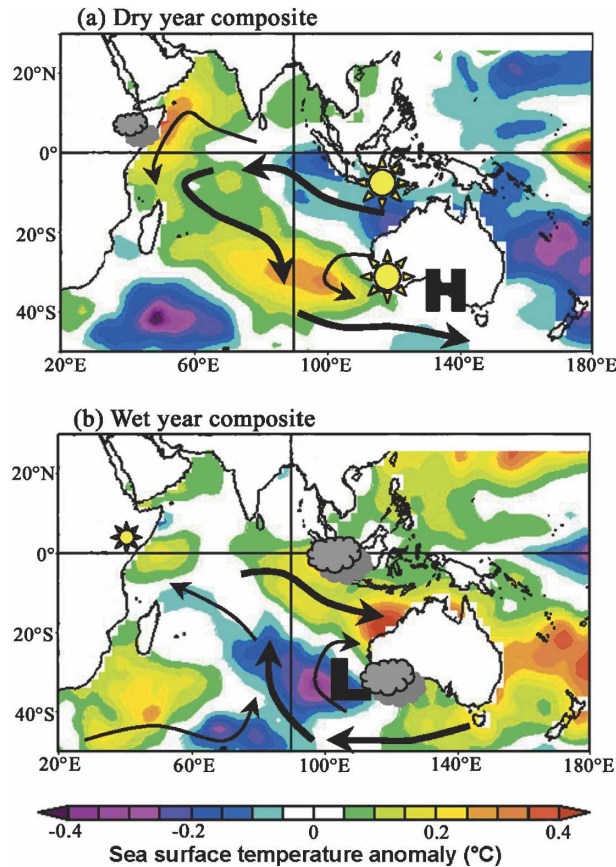


FIG. 15. Schematic diagram showing the connection between Indian Ocean climate variability and (a) dry and (b) wet years over SWWA. SST anomalies are shown as actual composite fields as in Fig. 5 (color shaded in $^{\circ}\text{C}$). Wind anomalies are shown schematically as bold arrows, pressure anomalies are indicated by H (high) and L (low), and rainfall anomalies are shown using sun/cloud symbols.

ingly similar composite anomaly patterns as those seen in the observations. The proposed dynamics linking large-scale Indian Ocean climate to SWWA rainfall extremes, as derived from the reanalysis data, appear robust in the coupled model. In particular, composite model patterns of Indian Ocean winds, rainfall, and SST are remarkably similar to those seen in the reanalyses and observations. The model anomalies have smaller magnitudes than in the reanalysis fields, which is likely due to a combination of the coarse model resolution, the model flux adjustment terms, and the fact that we composite ~ 150 events for each of the dry and wet years. We had initially assumed that the model would be too coarse in resolution to capture the dynamics of interannual rainfall variability over SWWA. However, given the close correspondence between composite climate patterns in the coupled model and the observed (both on the annual average as well as

during their seasonal evolution), and given that these features are basin-scale in their extent, it appears that the model is resolving regional southeast Indian Ocean climate variability rather well. Indeed, the finding that the model agrees with the observed, despite its coarse resolution, is symptomatic of the fact that the driving mechanisms for SWWA rainfall variability are large in scale.

An analysis of the seasonal evolution of SST, winds, and SLP during wet and dry years revealed a progressive amplification of anomalies toward a wintertime peak during JJA. In both the model and observed, ocean temperature anomalies can begin to develop as early as summertime, with an SST dipole appearing at P1 and P2 in the composite mean DJF conditions. Wind anomalies then develop during the ensuing months, amplifying to a pronounced large-scale acceleration (deceleration) of the Indian Ocean mean anticyclone by wintertime during dry (wet) years. The wind anomalies act to reinforce the SST anomalies via Ekman transport at P1 and air-sea fluxes at P2, yielding peak amplitude SST anomalies during JJA. Both the model and observed extreme years exhibit this seasonally evolving climate signal over the Indian Ocean: genesis in SST as early as summertime, rapidly increasing to maximum amplitude in atmospheric circulation and SST during winter (the season of highest SWWA rainfall), and then gradually abating during austral spring.

Because there is evidence of a net decrease in wintertime SWWA rainfall since the mid-1970s relative to the pre-1975 period (e.g., IOCI 2002), it is of interest to briefly assess whether recent multidecadal trends in SST and SLP bear any resemblance to the dry-year composite fields obtained in our study. We have plotted the JJA difference in SST and SLP during the 25-yr period 1980–2004 relative to 1951–75 in Fig. 16. The change in SLP is dominated by a positive trend in the Southern Annular Mode, associated with an intensification of the subtropical westerly winds. In addition, a large-scale increase in SLP has occurred at subtropical latitudes, with changes of up to 1.4 mb centered over Western Australia—of the same sign and of higher magnitude than the SLP anomaly seen during dry years in Fig. 3a. The changes in SST during 1980–2004 relative to 1951–75 show a pronounced warming over the Indian Ocean, with peak magnitude near pole P2, and cooling near pole P3—that is, temperature trends of the same sign as the characteristic SST anomaly pattern found during dry years (Fig. 5a). However, the observed temperature at P1 has warmed as well, so that the P1–P2 dipole is only $\sim 0.3^{\circ}\text{C}$ more pronounced during 1980–2004 as compared to the pre-1975 period.

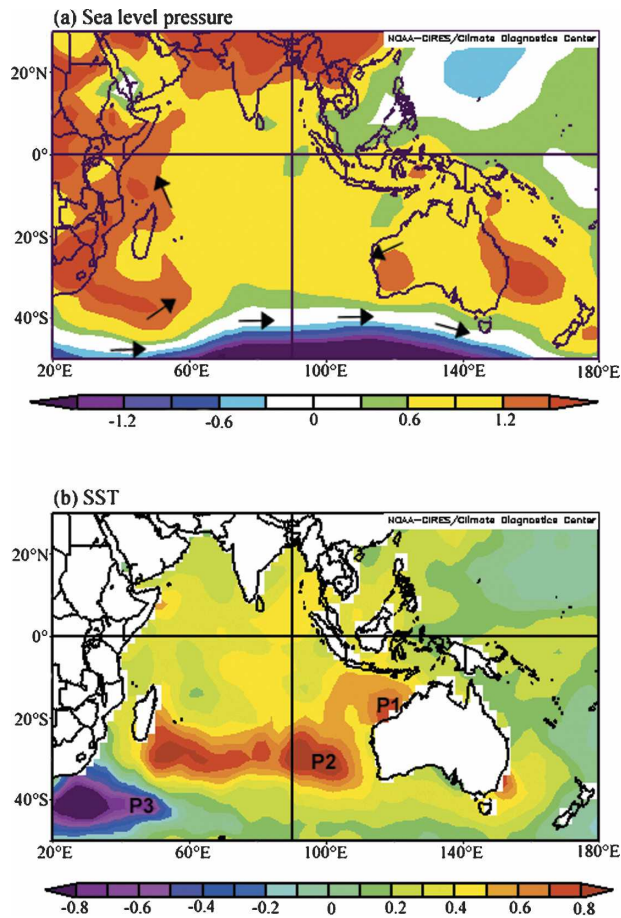


FIG. 16. Difference in the climatological mean wintertime (JJA) (a) SLP (mb) and (b) SST ($^{\circ}\text{C}$) during 1980–2004 relative to 1951–75. Geostrophic wind directions are indicated in (a) and the locations of poles P1–P3 are shown in (b).

With greater warming at P2 than at P1, the sense of this SST trend at the P1–P2 dipole should favor drier conditions over SWWA. In summary, there is some evidence that the post-1970 decrease in wintertime SWWA rainfall has been accompanied by a trend toward the dry-year scenario described in this paper. This is consistent with the proposed decadal modulation of the IOD noted by Ashok et al. (2004a). However, other factors, such as the documented positive trend in the Southern Annular Mode, are perhaps also playing a dominant role (e.g., see analysis in Karoly 2003).

The observed relationship between SWWA rainfall and Indian Ocean winds and SST might be modulated by other phenomena, such as ENSO and the ACW. While we did not establish a direct link between ENSO-related variability and SWWA precipitation, there are numerous climate teleconnections from the Pacific Ocean to the Indian Ocean, and so an indirect ENSO influence is quite likely. For example, the Indonesian

throughflow is thought to directly influence Indian Ocean variability (Lee et al. 2002; Xie et al. 2002), thereby likely affecting IOD characteristics (Saji and Yamagata 2003b) as well as the heat content at pole P1. The sensitivity of the Indonesian throughflow to ENSO (Meyers 1996; Behera et al. 2000; England and Huang 2005) means that it is likely that the climate of the tropical Pacific Ocean will impact SWWA rainfall via the Indian Ocean connection established in our study. There is anecdotal evidence for this, with several of the dry years coinciding with ENSO years in both the observations and the coupled climate model. However, in both the modeled and observed, the influence of ENSO on SWWA rainfall is much less obvious than the Indian Ocean connection, and quite possibly an artifact of the IOD–ENSO link.

The suggestion that the ACW impacts on Australian rainfall (White 2000) was not apparent in this study for the localized SWWA region. In particular, we observed no clear circumpolar propagation of anomalies leading up to anomalous SWWA rainfall years in either the model or reanalysis data. In spite of this, we cannot exclude the possibility that the pressure field across the south Indian Ocean is in some way responding to oscillations associated with the ACW or the Southern Annular Mode. Large-scale changes in extratropical air pressure affect the location and intensity of the subpolar westerlies, which in turn control SST and moisture advection near SWWA. Separating this extratropical forcing from the tropical and subtropical signals described in this paper is difficult as they are ultimately linked via the anticyclonic pressure system over the Indian Ocean. We have shown how interannual rainfall extremes over southwest Western Australia are linked to large-scale ocean–atmosphere variability over the Indian Ocean. Future work should address the formation and evolution of these ocean–atmosphere anomalies with a view to improving predictability of rainfall extremes in the region.

Acknowledgments. Access to historical data from the NCEP–NCAR reanalysis project and its graphical representation was provided by the Climate Diagnostics Center (CDC) at Boulder, Colorado, and obtained via the Web site <http://www.cdc.noaa.gov>. Observational rainfall data were provided by the Australian Bureau of Meteorology courtesy of Scott Power. We thank Barrie Hunt for access to 1000 yr of data from a 10 000-yr integration of the CSIRO coupled climate model. Chris Reason, Saji Hameed, and two anonymous reviewers provided helpful comments on an earlier draft of the manuscript. This research was supported by the Australian Research Council.

REFERENCES

- Allan, R. J., and M. R. Haylock, 1993: Circulation features associated with the winter rainfall decrease in southwestern Australia. *J. Climate*, **6**, 1356–1367.
- Ansell, T., C. J. C. Reason, and G. Meyers, 2000a: Variability in the tropical southeast Indian Ocean and links with southeast Australian winter rainfall. *Geophys. Res. Lett.*, **27**, 3977–3980.
- , —, I. N. Smith, and K. Keay, 2000b: Evidence for decadal variability in Southern Australian rainfall and relationships with regional pressure and sea surface temperature. *Int. J. Climatol.*, **20**, 1113–1129.
- Ashok, K., Z. Guan, and T. Yamagata, 2001: Impact of the Indian Ocean dipole on the relationship between Indian monsoon rainfall and ENSO. *Geophys. Res. Lett.*, **28**, 4499–4502.
- , —, and —, 2003a: A look at the relationship between the ENSO and the Indian Ocean dipole. *J. Meteor. Soc. Japan*, **81**, 41–56.
- , —, and —, 2003b: Influence of the Indian Ocean dipole on the Australian winter rainfall. *Geophys. Res. Lett.*, **30**, 1821, doi:10.1029/2003GL017926.
- , W.-L. Chan, T. Motoi, and T. Yamagata, 2004a: Decadal variability of the Indian Ocean dipole. *Geophys. Res. Lett.*, **31**, L24207, doi:10.1029/2004GL021345.
- , Z. Guan, N. H. Saji, and T. Yamagata, 2004b: Individual and combined influences of the ENSO and Indian Ocean Dipole on the Indian summer monsoon. *J. Climate*, **17**, 3141–3155.
- Behera, S. K., and T. Yamagata, 2001: Subtropical SST dipole events in the southern Indian Ocean. *Geophys. Res. Lett.*, **28**, 327–330.
- , P. S. Salvekar, and T. Yamagata, 2000: Simulation of interannual SST variability in the tropical Indian Ocean. *J. Climate*, **13**, 3487–3499.
- Black, E., 2003: The impact of Indian and Pacific Ocean processes on the East African short rains. *CLIVAR Exchanges*, Vol. 8, Nos. 2–3, International CLIVAR Project Office, Southampton, United Kingdom, 40–42.
- Cai, W., M. Collier, P. Durack, H. Gordon, A. C. Hirst, S. P. O'Farrell, and P. H. Whetton, 2003: The response of climate variability and mean state to climate change: Preliminary results from the CSIRO MK3 coupled model. *CLIVAR Exchanges*, Vol. 8, No. 4, International CLIVAR Project Office, Southampton, United Kingdom, 8–11.
- Drosowsky, W., 1993a: An analysis of Australian seasonal rainfall anomalies: 1950–1987. II: Temporal variability and teleconnection patterns. *Int. J. Climatol.*, **13**, 111–149.
- , 1993b: Potential predictability of winter rainfall over southern and eastern Australia using Indian Ocean sea-surface temperature anomalies. *Aust. Meteor. Mag.*, **42**, 1–6.
- England, M. H., and F. Huang, 2005: On the interannual variability of the Indonesian throughflow and its linkage with ENSO. *J. Climate*, **18**, 1435–1444.
- Frederiksen, C. S., and R. C. Balgovind, 1994: The influence of the Indian-Ocean Indonesian SST gradient on the Australian winter rainfall and circulation in an atmospheric GCM. *Quart. J. Roy. Meteor. Soc.*, **120**, 923–952.
- Gentili, J., 1991: Homologous peri-oceanic west coast climates in the Southern Hemisphere. *J. Roy. Soc. Western Aust.*, **74**, 15–33.
- Gordon, H. B., and S. P. O'Farrell, 1997: Transient climate change in the CSIRO coupled model with dynamical sea ice. *Mon. Wea. Rev.*, **125**, 875–907.
- Hirst, A. C., S. P. O'Farrell, and H. B. Gordon, 2000: Comparison of a coupled ocean–atmosphere model with and without oceanic eddy-induced advection. Part I: Ocean spinup and control integrations. *J. Climate*, **13**, 139–163.
- Hunt, B. G., 2001: A description of persistent climatic anomalies in a 1000-year climatic model simulation. *Climate Dyn.*, **17**, 717–733.
- Iizuka, S., T. Matsuura, and T. Yamagata, 2000: The Indian Ocean SST dipole simulated in a coupled general circulation model. *Geophys. Res. Lett.*, **27**, 3369–3372.
- IOCI, 2002: Climate variability and change in southwest Western Australia. Indian Ocean Climate Initiative Panel, Perth, Western Australia, Australia, 34 pp.
- Janowiak, J. E., A. Gruber, C. R. Kondragunta, R. E. Livezey, and G. F. Huffman, 1998: A comparison of the NCEP–NCAR reanalysis precipitation and the GPCP rain gauge–satellite combined dataset with observational error considerations. *J. Climate*, **11**, 2960–2979.
- Kalnay, E., and Coauthors, 1996: The NCEP/NCAR 40-Year Reanalysis Project. *Bull. Amer. Meteor. Soc.*, **77**, 437–471.
- Karoly, D. J., 2003: Ozone and climate change. *Science*, **302**, 236–237.
- Lee, T., I. Fukumori, and D. Menemenlis, 2002: Effects of the Indonesian throughflow on the Pacific and Indian Oceans. *J. Phys. Oceanogr.*, **32**, 1404–1429.
- Li, C. Y., and M. Q. Mu, 2001: The influence of the Indian Ocean dipole on atmospheric circulation and climate. *Adv. Atmos. Sci.*, **18**, 831–843.
- Li, T., B. Wang, C.-P. Chang, and Y. Zhang, 2003: A theory for the Indian Ocean dipole–zonal mode. *J. Atmos. Sci.*, **60**, 2119–2135.
- Mann, M. E., and J. M. Lees, 1996: Robust estimation of background noise and signal detection in climate time series. *Climate Change*, **33**, 409–445.
- McBride, J. L., and N. Nicholls, 1983: Seasonal relationships between Australian rainfall and the Southern Oscillation. *Mon. Wea. Rev.*, **111**, 1998–2004.
- Meyers, G., 1996: Variation of Indonesian throughflow and the El-Niño–Southern Oscillation. *J. Geophys. Res.*, **101**, 12 255–12 263.
- , P. McIntosh, L. Pigot, and M. Pook, 2006: The years of El Niño, La Niña, and interactions with the tropical Indian Ocean. *J. Climate*, in press.
- Nicholls, N., 1989: Sea surface temperatures and Australian winter rainfall. *J. Climate*, **2**, 965–973.
- Pitman, A. J., G. T. Narisma, R. A. Pielke Sr., and N. J. Holbrook, 2004: Impact of land cover change on the climate of southwest Western Australia. *J. Geophys. Res.*, **109**, D18109, doi:10.1029/2003JD004347.
- Power, S., F. Tseitkin, S. Torok, B. Lavery, R. Dahni, and B. McAvaney, 1998: Australian temperature, Australian rainfall and the Southern Oscillation, 1910–1992: Coherent variability and recent changes. *Aust. Meteor. Mag.*, **47**, 85–101.
- Qian, W. H., H. R. Hu, Y. Deng, and J. W. Tian, 2002: Signals of interannual and interdecadal variability of air–sea interaction in the basin-wide Indian Ocean. *Atmos.–Ocean*, **40**, 293–311.
- Rao, S. A., S. K. Behera, Y. Masumoto, and T. Yamagata, 2002: Interannual subsurface variability in the tropical Indian Ocean with a special emphasis on the Indian Ocean dipole. *Deep-Sea Res.*, **49B**, 1549–1572.
- Reason, C. J. C., 1999: Interannual warm and cool events in the subtropical/mid-latitude South Indian Ocean region. *Geophys. Res. Lett.*, **26**, 215–218.
- , C. R. Godfred-Spenning, R. J. Allan, and J. A. Lindesay,

- 1998: Air-sea interaction mechanisms and low-frequency climate variability in the South Indian Ocean region. *Int. J. Climatol.*, **18**, 391–405.
- Saji, N. H., and T. Yamagata, 2003a: Possible impacts of Indian Ocean dipole mode events on global climate. *Climate Res.*, **25**, 151–169.
- , and —, 2003b: Structure of SST and surface wind variability during Indian Ocean dipole mode events: COADS observations. *J. Climate*, **16**, 2735–2751.
- , B. N. Goswami, P. N. Vinayachandran, and T. Yamagata, 1999: A dipole mode in the tropical Indian Ocean. *Nature*, **401**, 360–363.
- , T. Ambrizzi, and S. E. T. Ferraz, 2005: Indian Ocean Dipole Mode events and austral surface temperature anomalies. *Dyn. Atmos. Oceans*, **39**, 87–101.
- Smith, I. N., P. McIntosh, T. J. Ansell, C. J. C. Reason, and K. McInnes, 2000: Southwest Western Australian winter rainfall and its association with Indian Ocean climate variability. *Int. J. Climatol.*, **20**, 1913–1930.
- Suzuki, R., S. K. Behera, S. Iizuka, and T. Yamagata, 2004: Indian Ocean subtropical dipole simulated using a coupled general circulation model. *J. Geophys. Res.*, **109**, C09001, doi:10.1029/2003JC001974.
- Walland, D. J., S. B. Power, and A. C. Hirst, 2000: Decadal climate variability simulated in a coupled general circulation model. *Climate Dyn.*, **16**, 201–211.
- White, W. B., 2000: Influence of the Antarctic Circumpolar Wave on Australian precipitation from 1958 to 1997. *J. Climate*, **13**, 2125–2141.
- Xie, P., and P. A. Arkin, 1996: Analyses of global monthly precipitation using gauge observations, satellite estimates, and numerical model predictions. *J. Climate*, **9**, 840–858.
- Xie, S.-P., H. Annamalai, F. A. Schott, and J. P. McCreary Jr., 2002: Structure and mechanisms of South Indian Ocean climate variability. *J. Climate*, **15**, 864–878.
- Yamagata, T., S. A. Behera, S. A. Rao, Z. Guan, K. Ashok, and H. N. Saji, 2003: Comments on “Dipoles, temperature gradients, and tropical climate anomalies.” *Bull. Amer. Meteor. Soc.*, **84**, 1418–1422.